Automatic Segmentation of White Matter Hyperintensities from Brain Magnetic Resonance Images in the Era of Deep Learning and Big Data – A Systematic Review

Ramya Balakrishnan†[1,3], Maria del C. Valdés Hernández†*[1,2], Andrew Farrall[1,2]

[1] Edinburgh Imaging Academy, University of Edinburgh, Edinburgh, UK

[2] Centre for Clinical Brain Sciences, University of Edinburgh, Edinburgh, UK

[3] International Institute of Health Sciences, Sri Lanka

*Corresponding author

† Equal contribution

Correspondence to: Dr. Maria del C. Valdés Hernández

        Centre for Clinical Brain Sciences

        Dementia Research Institute at The University of Edinburgh, Room FU427

        Chancellor's Building

        49 Little France Crescent

        Edinburgh, EH16 4SB, UK

e-mail: M.Valdes-Hernan@ed.ac.uk

White Matter Hyperintensities Segmentation Review

ABSTRACT

Background: White matter hyperintensities (WMH), of presumed vascular origin, are visible and quantifiable neuroradiological markers of brain parenchymal change. These changes may range from damage secondary to inflammation and other neurological conditions, through to healthy ageing. Fully automatic WMH quantification methods are promising, but still, traditional semi-automatic methods seem to be preferred in clinical research. We systematically reviewed the literature for fully automatic methods developed in the last five years, to assess what are considered state-of-the-art techniques, as well as trends in the analysis of WMH of presumed vascular origin.

Method: We registered the systematic review protocol with the International Prospective Register of Systematic Reviews (PROSPERO), registration number - CRD42019132200**.** We conducted the search for fully automatic methods developed from 2015 to July 2020 on Medline, Science direct, IEE Explore, and Web of Science. We assessed risk of bias and applicability of the studies using QUADAS 2.

Results: The search yielded 2327 papers after removing 104 duplicates. After screening titles, abstracts and full text, 37 were selected for detailed analysis. Of these, 16 proposed a supervised segmentation method, 10 proposed an unsupervised segmentation method, and 11 proposed a deep learning segmentation method. Average DSC values ranged from 0.538 to 0.93, being the highest value obtained from a deep learning segmentation method. Only four studies validated their method in longitudinal samples, and eight performed an additional validation using clinical parameters. Only 8/37 studies made available their method in public repositories.

Conclusions: Although deep learning methods reported highly accurate results, we found no evidence that favours them over the more established k-NN, linear regression and unsupervised methods in this task. Data and code availability, bias in study design and ground truth generation influence the wider validation and applicability of these methods in clinical research.

Keywords: White matter lesions, white matter hyperintensities, supervised segmentation, unsupervised segmentation, deep learning, FLAIR hyperintensities

INTRODUCTION

In 1987, Hachinski, Potter, and Merskey (Hachinski, Potter & Merskey, 1987) first used the term leukoaraiosis to describe abnormal findings observed in subcortical white matter on a brain computed tomography (CT) scan. Leukoaraiosis has been also referred to as white matter lesions (Inzitari, 2003). With increasing use of magnetic resonance imaging (MRI) as diagnostic tool, leukoaraiosis has been increasingly referred to as white matter hyperintensities (WMH) (Wardlaw et al., 2013), due to their hyperintense appearance on T2-weighted sequences. WMHs have been associated with reduced cognitive functions, dementia, gait, balance, mobility, and mood disorders (Fazekas & Wardlaw, 2013; Zheng, Delbaere, Close, Sachdev & Lord, 2011). They have also been frequently observed in the asymptomatic aged population and in various common geriatric conditions such as cerebrovascular disease, cardiovascular disease, and dementia, as well as in multiple sclerosis, other autoimmune diseases and psychiatric disorders such as depressive disorder, bipolar disorder and schizophrenia (Kim, MacFall & Payne, 2008; Rachmadi et al., 2018). WMH prevalence in the general population ranges from 11 – 21% in adults aged around 64 and increases with age to 94% at age 82 (Debette & Markus, 2010). One study reported that among elderly population aged 60 to 90 years, 90% have WMH (Hasan et al., 2019).

Detailed WMH evaluation for number, volume, location, and distribution on MRI may provide crucial information on aetiology, prognosis, and progression of various diseases; their accurate quantification may help measure treatment effectiveness (Manjón et al., 2018; Qin et al., 2018). WMH severity is considered an indirect marker of normal appearing white matter integrity and a surrogate marker of small vessel disease (SVD) (Maltais et al., 2019; Maniega et al., 2015). With the advance of MRI technology, several methods have been developed to quantify WMH volumes through image segmentation, "a process which typically partitions the

spatial domain of an image into mutually exclusive subsets called regions, each one of which is uniform and homogeneous with respect to some property such as tone or texture and whose property value differs in some significant way from the property value of each neighbouring regions" (Haralick et al., 1991). However, WMH are not homogeneous, have ill-defined boundaries and their tone and texture may not significantly differ from their neighbouring tissues. Biologically, they represent the "tip of the iceberg" of demyelinating, inflammatory processes that affect the whole brain and which are reflected in the many neuroradiological features, accompanying and sometimes coalescing with them. The essence of digital image segmentation is to recognise edges which separate WMH from "background". The degree of subjectivity in WMH identification and boundary recognition, challenge WMH segmentation, leading to low agreement in reported studies of manual delineation of WMH ground truth segmentations (Akudjedu et al., 2018; Despotović, Goossens & Philips, 2015; Keller & Roberts, 2009).

Unlike normal tissues, for which validated fully automatic protocols exist and have become standard, a robust method for WMH segmentation has yet to emerge. Clinical research groups usually select a WMH segmentation method based on their own capabilities, existing methods' specifications, availability and sustainability of the source code, and image acquisition protocols. Then, groups adapt these methods in-house and validate them for the specific study protocol. Normal tissue intensities follow a normal distribution, but abnormalities do not. In the specific case of WMH, signal intensity and spatial distributions vary, displaying unique signatures for each disease and cohort. Table 1 summarises some WMH signatures in normal ageing, SVD, Alzheimer's disease, multiple sclerosis (MS) and vanishing white matter disease - an autosomal recessive disorder (Labauge et al., 2009). In addition to specific disease/neurological condition characteristics, there is a wide spectrum of variation in WMH appearances in individuals from different disease groups (Figure 1).
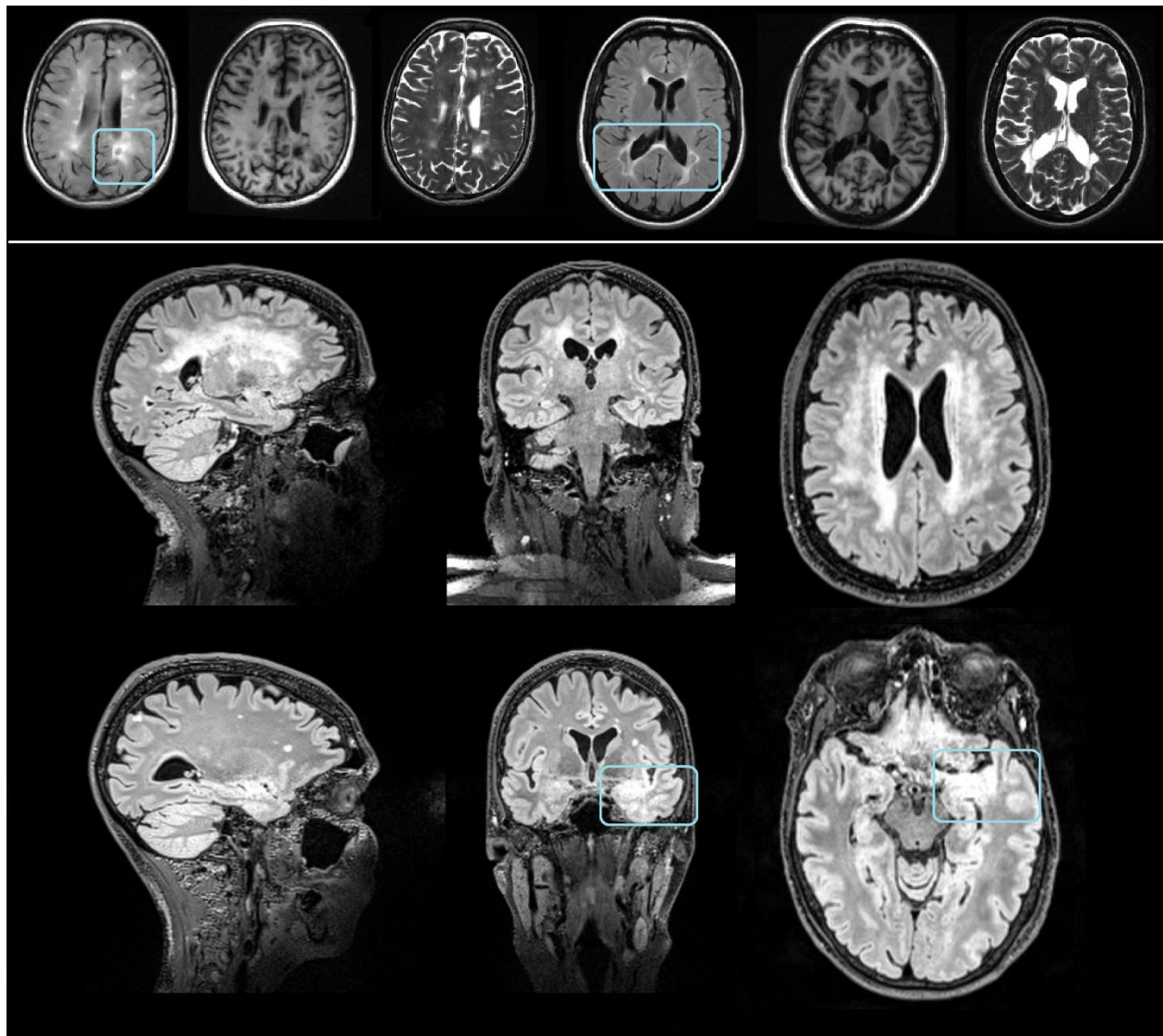
Figure 1. T2-hyperintensties in Multiple Sclerosis (top row) and sporadic Small Vessel Disease (middle and bottom rows). Top row: Representative axial slice from two MS patients displayed, from left to right, in FLAIR, T1-weighted and T2-weighted MRI at 1.5T, showing pseudocavitated FLAIR hyperintense lesions (enclosed in rectangles). Middle row: From left to right, sagittal, coronal and axial views of a FLAIR 3T MRI scan from a patient with SVD and a high burden of WMH of presumed vascular origin. Bottom row: From left to right, sagittal, coronal and axial views of a FLAIR 3T MRI scan displaying a large confounding image artefact (enclosed in rectangles in coronal and axial views) from a patient with SVD with a low burden of WMH of presumed vascular origin.

WMHs arising as a result of infections (e.g. viral, bacterial), can overlay those which already exist due to other processes (e.g., normal ageing) or comorbidities (e.g., SVD): this poses a challenge for their differential identification and segmentation. For example, in CoVID-19 patients, in addition to large vessel strokes, WMHs have been reported bilaterally in the thalami, cerebellum and temporal lobes, and also in the corpus callosum along with abnormal T2 signal in the olfactory bulb and microbleeds in the thalami (Imaging in COVID-19 complications - ESR Connect, 2020). In these brain regions, WMH commonly found in the elderly are uncommon. Symmetric frontal WMH and cortical hyperintensities have been reported in other COVID-19 patients with more severe respiratory disease status (MRI Shows Brain Abnormalities in Some COVID-19 Patients, 2020) along with punctate cortical blooming artefacts. But influence of treatment, comorbidities and disease severity make it difficult even for neuroradiologists to identify specific disease-related patterns that could differentially aid in diagnosis and patient stratification.

Table 1. Neuroradiological signatures of T2 white matter hyperintensities in normal ageing, SVD, Alzheimer's disease, multiple sclerosis and vanishing white matter disease.

	Normal ageing	**SVD**	**Alzheimer's disease**	**Multiple sclerosis**	**Vanishing white matter disease**
Extent	Range from thin periventricular lining to confluent regions in the deep white matter	Range from periventricular with few spots in the deep white matter to confluent regions	Thin periventricular lining with spots in the deep white matter	Range from periventricular with few spots in the deep white matter to large regions that can enclose "pseudocavities" of low T1 signal, also referred as "cavitary lesions" (Ayrignac et al., 2016)	Large and confluent enclosing "pseudocavities" of low T1 signal, also referred as "cavitary lesions" (Ayrignac et al., 2016)

White Matter Hyperintensities Segmentation Review

Characteristic brain regions	Non-specific Disseminated throughout the periventricular and deep white matter and corpus striatum. Gradual progression extending from the periventricular starting from frontal and parietal regions. Rare in the temporal lobes, brain stem and cerebellum	Non-specific Disseminated throughout the periventricular and deep white matter, corpus striatum and thalami. Rare in the cerebellum	Non-specific. Disseminated throughout the white and deep grey matter. Rare in juxtacortical regions	Disseminated throughout the whole brain, including midbrain, brainstem, juxtacortical regions, corpus callosum and cerebellar peduncles	Disseminated throughout the whole brain. External capsule and corpus callosum diffusely involved
Symmetry between brain hemispheres	Symmetric distribution	Symmetric distribution	Symmetric distribution	Symmetric distribution in the cerebrum, but not in the cerebellum	Symmetric distribution
Histogram distribution in FLAIR MRI	Tail (from normal white matter) fits Extreme Value distributions (e.g. Fréchet or Gumbel)	Tail (from normal white matter) fits Extreme Value distributions (e.g. Fréchet or Gumbel). Laplacian distribution can be observed in some cases if/when strokes	Very skewed distribution independent (i.e. separated) from that of the normal white matter	Bimodal distribution independent (i.e. separated) from that of the normal white matter (considering cavitation).	Bimodal distribution independent (i.e. separated) from that of the normal white matter (considering cavitation)

		are considered part of the hyperintensities			
Signatures	"cotton-wool" appearance	"cotton-wool" appearance combined with subtle hyperintense large areas, or overt and confluent with irregular patterns	"cotton-wool" appearance. Confluent regions are uncommon	Juxtacortical lesions, lesions in corpus callosum perpendicular to the ventricular linings known as "Dawson fingers", cavitary lesions predominantly periventricular, punctate asymmetrical lesions involving the posterior fossa	Diffuse involvement of the corpus callosum Symmetric involvement of the cerebellum and middle cerebellar peduncles. Cavitary lesions have an anterior predominance
Presence of other features	Perivascular spaces (from none to mild) and possibly lacunar lesions and/or reminiscences of previous mild ischaemic strokes	Perivascular spaces, lacunes, ischaemic strokes and few microbleeds	Marked brain atrophy and hippocampal sclerosis		
Borders	Not well defined	Not well defined	Better defined than in SVD or healthy ageing	Better defined than in SVD or healthy ageing (Griffanti et al.2016)	Not well defined

To help in the selection of the WMH segmentation methods and discuss their applicability, other systematic literature reviews have been published, but on focused topics specific to diseases, e.g. MS lesion segmentation (García-Lorenzo et al., 2013; Llado et al., 2011, 2012; Miller et al., 1998; Mortazavi, Kouzani & Soltanian-Zadeh, 2012). Methods which work for MS may perform moderately if applied to individuals with SVD or normal elderly (Table 1). Caligiuri et al. conducted a systematic review on fully automated methods used for segmenting WMH in normal ageing and patients with vascular pathology and risk factors, covering the years 1980 – 2014 (Caligiuri et al., 2015). Two other non-overlapping reviews (Wardlaw et al., 2015; Blair et al., 2017) discussed different approaches, published up to 2016, not only for segmenting WMH, but also for assessing other neuroimaging markers of SVD. Another study that systematically reviewed the machine-learning methods developed to differentiate healthy aging from different types of dementia (Pellegrini et al., 2018) included studies aimed at detecting and segmenting WMH in ageing and dementia published in the years from 2006 until September 2016. The last five years (i.e., since 2015) have seen a boost in sample sizes, computational power and the introduction / application of deep learning in clinical research, in parallel with an increase in high-quality imaging acquisitions, facilitated by 3T MRI scanners. We systematically reviewed the literature in this period to analyse and inform on the fully automatic computational methods developed to segment WMH of presumed vascular origin, aiming to offer an overview of the state-of-art in the field.

METHODS

This systematic review protocol is registered on the International Prospective Register of Systematic Reviews (PROSPERO), registration number - CRD42019132200 (2020) to avoid unintended duplication and to aid in transparent reporting. The search was conducted from

January 2015 to July 2020 on Medline, Science direct, IEE Explore and Web of Science. For each database, we developed a search strategy to retrieve as many WMH segmentation method articles as possible. We identified keywords by expanding the subject components from the review question: white matter lesion, white matter hyperintensities, leukoaraiosis, aging, WMH, segmentation, supervised segmentation, unsupervised segmentation, machine learning, deep learning, parcellation, artificial neural network, pattern recognition, clustering, classification, magnetic resonance imaging, MRI. We applied language restriction and age limit (45 plus years) for Medline. We summarize search strategy details for each database in Appendix 1. We imported all articles retrieved into the reference manager Mendeley, and removed all duplicates. We then screened abstracts and titles to exclude studies outwith the scope of the review. Then we evaluated the full text of the remaining articles, applying inclusion and exclusion criteria (explained below). We also reviewed references of these articles for possible papers missed in the primary search.

Additionally, the following journals were hand-searched to identify the articles that presented a method for segmenting WMH in the period covered by this review.

1.   Neuroimage – used keywords WMH and Segmentation from January 2015 until July 2020: 6 journal articles identified matched with the search results (100% recall).

2.   NeuroImage Clinical – searched from January 2015 until July 2020 : Identified 7 articles which matched the search results. Hence, recall rate is 100%

3.   Neuroinformatics - used keywords WMH and Segmentation. Searched from January 2015 until July 2020: Found 2 articles which matched the search results (100% recall).

Inclusion and Exclusion Criteria

Inclusion criteria

White Matter Hyperintensities Segmentation Review

- Presentation and/or validation of a fully automated method for segmenting WMH of presumed vascular origin from human brain MR images from January 2015 to July 2020
- Studies published in English

Exclusion criteria

- Animal studies
- Segmentation methods solely for multiple sclerosis (MS) lesions or validated using only data from MS patients
- No description of new fully automated segmentation method
- Evaluation of segmentation method accuracy on CT images
- Segmentation of brain regions, brain tumours or other pathologies that are not WMH of presumed vascular origin
- Semi-automated segmentation methods
- No information on segmentation method similarity metrics used or no evaluation against ground truth segmentations
- Focus on pre-processing or classification of MR images
- Methods designed for assessment of WMH evolution (i.e. longitudinal analysis) without cross-sectional validation of their results
- Insufficient information to replicate or apply the segmentation method
- Studies published only as abstracts
- Articles on conference proceedings
- No description of the segmentation method of WMH of presumed vascular origin

Assessment of Methodological Quality

We evaluated the methodological quality of each study using QUADAS 2: a tool to assess the risk of bias and the applicability of the methods / procedures (https://www.bristol.ac.uk/media-

library/sites/quadas/migrated/documents/quadas2.pdf). QUADAS 2 contains four domains: 1) patient selection; 2) index test; 3) reference test; and 4) flow and timing. In our case, index text refers to WMH segmentation method/algorithm. Different to the original QUADAS 2 questionnaire, the evaluation of the index text consisted in assessing whether or not the reference standard was used in any way by the segmentation method. We completed the online form for each of the included studies. If a study were judged low in all four domains in relation to bias or applicability from answering the specific questions from each domain, then it was considered as "low risk of bias". If a study were judged high or unclear for one or more domains, then it was considered as "risk of bias" or as having concerns regarding applicability.

DATA EXTRACTION

From the included papers, we extracted the following data:

- Title, year of publication, journal name, study design
- Number of subjects or images, age, gender
- Patient selection criteria, sample size
- Type of MRI sequences used (details about the scanner used)
- Information on imaging features used for investigation
- Details about pre-processing steps (registration, brain extraction, intensity inhomogeneity correction, noise reduction, intensity normalization)
- Method to remove false positives
- Reference standard(s)
- Segmentation method details
- Non-imaging features used for clinical correlation with WMH volume (e.g., cognitive test)
- Sensitivity, specificity, accuracy, dice similarity index, false negative ratio (FNR) and false positive ratio (FPR) of the proposed segmentation method
- Visual rating scale used for validating the segmentation method (if any)

Extracted data were tabulated, synthesized, and evaluated for methodological flaws and applicability of the proposed techniques.

RESULTS

Search Results

The online literature search yielded 2327 papers after removing 104 duplicate citations. The selection process, conducted according to the Preferred Reporting Items for Systematic Reviews and Meta-Analyses (PRISMA), is schematically represented in Figure 2. We removed 2268 papers after screening titles and abstracts, leaving 59 papers for full text screening. We excluded further 19 papers for these reasons: validated the method using datasets with brain tumours (2 studies) or MS patients only (6 studies), method for segmenting lacunes instead (1 study), method for segmenting perivascular spaces (3 studies) or only small T2 hyperintensities (1 study), full text not available (1 study), sample size less than 20 (1 study), presented a tool for displaying and not segmenting WMH (1 study), modelling WMH distribution (1 study), or only quantifying longitudinal change (1 study). Also, three studies did not propose a new segmentation method of WMHs but compared the performance of existing machine learning based segmentation methods of WMHs (Dadar et al., 2017b; Kuijf et al., 2019; Rachmadi, Valdés-Hernández, Agan & Komura 2017), leaving 37 studies for full analysis.

White Matter Hyperintensities Segmentation Review
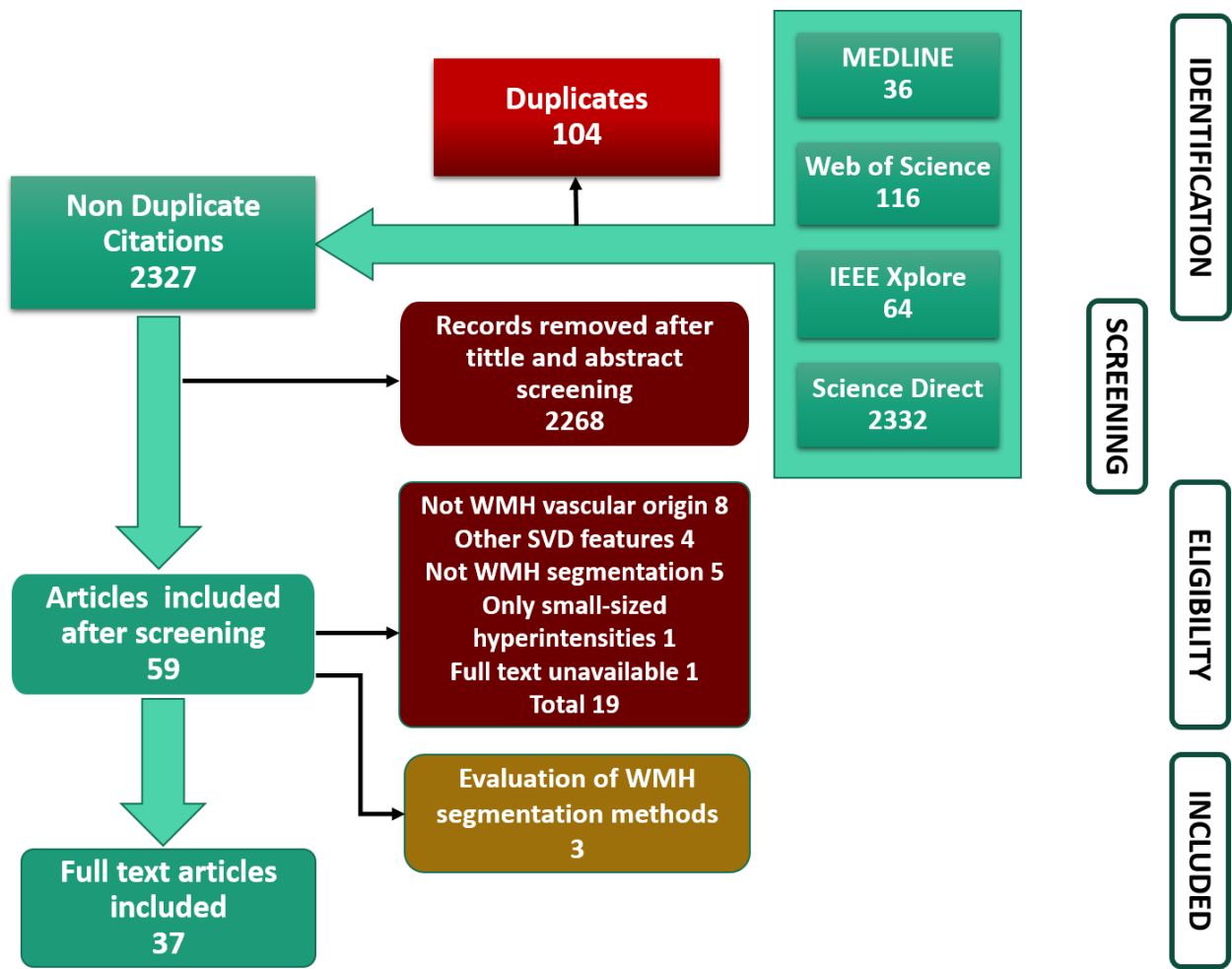
Figure 2. PRISMA Flow diagram of the systematic literature search.

Sample Characteristics

The 37 studies included analysed imaging data from approximately 7000 individuals. The exact number and quantitative breakdown of sample characteristics was not possible to ascertain because several studies used overlapping publicly available datasets lacking accompanying clinical or demographic metadata. One large-scale multicentre study involved 2781 subjects from 12 different cites (Schirmer et al., 2019). Samples involving more than 500 individuals were analysed in only two other studies (Griffanti et al., 2016 (n=559); Jiang et al., 2018 (n=566)). Eight studies used small relevant samples (i.e., fewer than 30 individuals with WMH of presumed vascular origin) (Ding et al., 2020; Rachmadi et al., 2020; Rincón et al. ,2017; Roy et

al., 2015; Stone et al., 2016, Van Opbroek et al., 2015a, 2015b; Valverde et al., 2017). Three of them used, in addition, data from MS patients (Rachmadi et al., 2020; Van Opbroek et al., 2015a, 2015b). Fourteen studies validated their results in data provided by Medical Image Computing and Computer Assisted Intervention (MICCAI) segmentation challenges (Roy et al., 2015; Sudre et al., 2015; Van Obproek et al., 2015a, 2015b; Wang et al, 2015; Valverde et al., 2017; Zhan et al., 2017; Knight et al., 2018; Li et al., 2018; Manjón et al., 2018; Moeskops et al., 2018; Sundaresan et al., 2019; Wu, Zhang, Wang & Tang, 2019; Liu et al., 2020). Nine of them also used additional datasets or patient data from clinics. Out of 37, twelve studies reported using data from prospective studies or clinics (Atlason et al., 2019; Bowles et al., 2017; Guerrero et al., 2017; Hong et al., 2020; Moeskops et al., 2018; Ling et al., 2018; Park et al., 2018; Qin et al., 2018; Rincón et al., 2017; Roy et al., 2015; Sundaresan et al., 2019; Wang et al., 2015). Four studies used data from the Alzheimer's Disease Neuroimaging Initiative (ADNI) (Sudre et al., 2017; Dadar et al., 2017a; Rachmadi et al., 2018, 2020), of which only two declared the subset used (Rachmadi et al., 2018, 2020). Two studies recruited patients diagnosed with migraine (Hong et al., 2020; Park et al., 2018). We summarized the characteristics of the samples in the included articles in Table 2.

Table 2: Sample characteristics, type of segmentation algorithm proposed and average spatial agreement with reference segmentations in the relevant dataset used, from the 37 studies reviewed. Studies appear in alphabetical order of the first author's surname by year of publication.

STUDY / CODE REPOSITORY	SAMPLE SIZE	SAMPLE CHARACTERISTICS	SEQUEN-CES AND FIELD STRENGTH	TYPE OF SEGMENTA-TION	AVERAGE SPATIAL AGREEMENT WITH REFERENCE SEGMENTATION
Roy et al. (2015)	24 Additio-nal eval. in data	Selected from a larger cohort of elderly subjects with hypertension based on the burden of WMH. Further evaluation in data from 20 MS patients from the MICCAI MS Segmentation Challenge II	T1W, FLAIR / 1.5T	Supervised	DSC 0.60 - 0.76 In MS patients: DSC 0.42, TPR 0.55, PPV 0.38

White Matter Hyperintensities Segmentation Review

	from n=20	2008 (https://www.nitrc.org/projects/msseg)			
Sudre et al. (2015)	Not especi-fied	Simulated data from the BrainWeb project (Kwan, Evans & Pike, 1999), MS patient data from https://www.nitrc.org/projects/msseg and data with age-related WMH from the MICCAI BrainS challenge	T1W, FLAIR / 1.5T	Unsupervi-sed	DSC 0.46, FPR 0.1, TPR 0.38, FNR 0.62
Van Opbroek et al. (2015a)	40	20 healthy elderly subjects from the Rotterdam scan study and 20 MS patients from https://www.nitrc.org/projects/msseg	T1W, T2W/PD, FLAIR / 1.5T	Supervised	Total accuracy score 78%, TPR 42.3 & 52.7 %, FPR 73.2 & 70.0 %
Van Opbroek et al. (2015b)	40	20 healthy elderly subjects from the Rotterdam scan study and 20 MS patients from https://www.nitrc.org/projects/msseg	T1W, T2W/PD, FLAIR / 1.5T	Supervised	-
Wang et al. (2015)	60 +	Elderly patients scanned as part of normal patient care, aged 61- 86 years (mean age 68.2 years), with various degrees of vascular white matter abnormalities. Further evaluation used data from 10 MS patients from the MICCAI MS Segmentation Challenge II 2008 (https://www.nitrc.org/projects/msseg)	T1W, T2W, FLAIR / 1.5T & 3T	Unsupervi-sed	DSC 0.81-0.84, FPR 0.13-0.24, FNR 0.14-0.2 In MS patients: TPR 0.38-0.40, PPV 0.36-0.48
Zhan et al. (2015)	40	Patient selection process not provided, mean age 62.2 ± 5.9 years	T1W, T2W, FLAIR /1.5T	Unsupervi-sed	DSC 0.75, TPF 0.72, FPF 0.46
Damangir et al. (2016)	119	Patients from Kings Health Partners- Dementia Case Register with AD, MCI, and healthy controls, aged 76.4 ± 7.4 years, 56% Females	T1W, T2W, FLAIR, PD / 1.5T	Unsupervi-sed	DSC 0.85 – 0.91
Griffanti et al. (2016) https://fsl.fmrib.ox.ac.uk/fsl/fslwiki/BIANCA	559	Selection criteria not provided. Dataset 1 (neurodegenerative cohort)- 85 patients Dataset 2 (vascular cohort)-MRI data from 474 consecutive patients	T1W, FLAIR / 3T	Supervised	DSC 0.76, FNR 0.25, FPR 0.22
Stone et al. (2016)	24	Traumatic brain injured patients aged 28-58 years (mean age 39.6 ± 8.1 years) with isolated traumatic lesions in the cerebral white matter, recruited based on potential concussive events	T1W, T2W, FLAIR / 3T	Supervised	Sensitivity 0.68, PPV 0.51
Bowles et al. (2017)	127	Selection criteria not provided. Heterogeneous dataset containing imaging data from three different acquisition protocols	T1W, T2W, FLAIR / 1.5T	Unsupervi-sed	DSC 0.70

White Matter Hyperintensities Segmentation Review

Dadar et al. (2017a)	130	Dataset 1: 80 subjects aged 70-90 years old with either normal cognition, MCI or AD. Dataset 2: 40 cognitively normal subjects at risk of AD aged 55-75 years Dataset 3: 10 subjects from ADNI2/GO selected to have different WMH burden	T1W, FLAIR / 1.5T & 3T	Supervised	DSC 0.51 - 0.62
Ghafoorian et al. (2017)	420	Subjects for the RUN DMC study aged between 50 and 85 years with cerebral SVD on neuroimaging (appearance of WMH and/or lacunes)	T1W, FLAIR / 1.5T	Deep learning	DSC 0.78-0.79
Rincón et al. (2017)	28	13 patients with cortical and lacunar ischemic infarctions, between 40 and 79 years of age, mini–mental state examination (MMSE) scores ≥ 23, no severe problems of language and visual/auditory neglect. 15 MCI patients meeting Petersen criteria.	T1W, FLAIR / 1.5T	Supervised	DSC 0.64
Sudre et al. (2017)	85 +	Two datasets of unspecified size: one from ADNI with minimal to none WMH load and other with a range of WMH burden. Additional Synthetic data derived from a non-specified number of data was used.	T1W, FLAIR / 3T	Unsupervised	DSC 0.2 – 0.7
Valverde et al. (2017) http://atc.udg.edu/nic/msseg	20	MRBrainS public database, selected with varying atrophy degrees and WMH loads	T1W, FLAIR / 3T	Unsupervised	TPF 0.7- 0.8
Zhan et al. (2017)	104	Dataset 1: 50 subjects from ACCORD-MIND mean age 62 years Dataset2: 54 image datasets from https://www.nitrc.org/projects/msseg	T1W, T2W, PD, FLAIR / 1.5T	Supervised	DSC 0.76, TPR 0.83
Bandeira Diniz et al. (2018)	91	Image data from a database with some of the volumes containing less than 10 lesions clusters while other volumes contains more than 100.	FLAIR / Acquisition details not provided	Deep learning	Sensitivity 78.79%, Specificity 98.77%
Guerrero et al. (2018)	167	Patients with their first clinically evident non-disabling lacunar or mild cortical ischemic stroke	T1W, FLAIR / 1.5T	Deep learning	DSC 0.607
Jiang et al. (2018) https://cheba.unsw.edu.au/research-	566	Data from two sources: 1) Sydney Memory and Ageing Study (n=166 aged 70 - 90 years old provided longitudinal data in 3 time points).	T1W, FLAIR / 1.5T & 3T	Supervised	DSC 0.85, Sensitivity 0.91, Specificity 0.99

Balakrishnan, Valdes-Hernandez and Farrall

groups/neuroim aging/pipeline		2) Older Australian Twins Study (n=400 aged 65 and above).			
Knight et al. (2018)	96	From 7 different sources, provided by different WMH and MS lesion segmentation challenges	FLAIR / 1.5T & 3T	Supervised	DSC 0.41-0.70
Li et al. (2018) https://github.c om/hongweilibr an/wmh_ibbmT um	170	WMH segmentation challenge dataset (https://wmh.isi.uu.nl/).	T1W, FLAIR / 1.5T & 3T	Deep learning	DSC 0.8, Recall 0.84
Ling et al. (2018)	156	CADASIL patients 18 years old and above. Mutation of gene NOTCH3 confirmed. 90 patients with 2D FLAIR images were aged 24–74 years, mean age 49 ± 11 years, F:M = 54:36. 66 patients with 3D FLAIR images were aged 35–81 years, mean age 57 ± 11 years, F:M = 46:20	T1W, FLAIR / 1.5T & 3T	Supervised	DSC 0.79 for 2D FLAIR images and 0.76 for 3D FLAIR images
Manjón et al. (2018)	128 +	128 subjects with a wide range of WMH load aged 38.6–92.1 years (M:F = 60:68) from Australian Imaging Biomarkers and Lifestyle (AIBL) study, and unspecified data from https://www.nitrc.org/projects/msseg	T1W, FLAIR / 1.5T & 3T	Deep learning	DSC 0.78
Moeskops et al. (2018)	226	Patient data from MRBrainS13 challenge and two other datasets: patients with type 2 diabetes mellitus, healthy controls and patients from memory clinic	T1W, FLAIR / 3T	Deep learning	DSC 0.67
Park et al. (2018) https://github.c om/bypark/DE WS	148	Diagnosis of migraine confirmed by two headache specialists mean age 44.4 (SD 12.4) years	T1W, FLAIR / 3T	Supervised	TPR 0.7-0.91
Qin et al. (2018)	88 (uses WM lesion 3D atlas from 277 FLAIR images)	Adults from mid to older ages with WMH without confounding radiological evidence of recent or old strokes	T1W, FLAIR / 1.5T	Supervised	DSC 0.65 - 0.67, Precision 0.68, Recall 0.68 - 0.69
Rachmadi et al. (2018)	288	ADNI subjects randomly selected. From the subsample with ground truth segmentations (n=20) 3 were cognitively	T1W, T2W, FLAIR / 3T	Deep learning	DSC 0.54

https://github.com/deepmedic/deepmedic		normal, 12 had early MCI and 5 had late MCI			
Atlason et al. (2019)	170	AGES-Reykjavik study. Age 66–93 years at first visit, and WMH segmentation challenge dataset (https://wmh.isi.uu.nl/).	T1W, T2W, FLAIR / 1.5T & 3T	Unsupervised	DSC 0.77, TPR 0.64 in AGES-Reykjavik dataset. DSC 0.53-0.67, TPR 0.25-0.40 in WMH segmentation challenge dataset
Schirmer et al. (2019)	2783	Acute ischaemic stroke patients ages 63.28 (SD 14.70) years, 61% male, 10.6% had a prior stroke	FLAIR / Field strength not specified	Deep learning	DSC 0.93
Sundaresan et al. (2019)	133	Five datasets: 1) Neurodegenerative cohort (n=21, age range 63–86 years, mean age 77.1 ±5.8 years F:M = 10:11) 2) Patients that recently experienced a minor non-disabling stroke or transient ischemic attack (n=18, (age range 50–91 years, mean age 73.27 ±12.32 years, F:M = 7:11) 3) CADASIL patients (n=15, age range 33–70 years, mean age 53.73 ±11.31 years, F:M = 11:4) 4) Healthy controls (n=19, age range 29–70 years, mean age 54.58 ±11.25 years, F:M = 6:13) 5) MICCAI WMH segmentation challenge dataset (n=60, selected from 3 different primary cohorts, https://wmh.isi.uu.nl/)	T1W, T2W, FLAIR / 1.5T & 3T	Supervised	DSC 0.77 TPR 0.73 – 0.98
Wu et al. (2019)	135	Data from BIOCARD study. Subjects either cognitively normal (n=113) or MCI (n=22), based on the (NIA/AA) research diagnostic criteria	T1W, FLAIR / 3T	Supervised	DSC 0.62, FPR 0.35, FNR 0.37
Wu, Zhang, Wang & Tang (2019)	60	Data from a MICCAI WMH challenge (https://wmh.isi.uu.nl/). Demographic data not provided	T1W, FLAIR / 1.5T & 3T	Deep learning	DSC 0.78, Recall 0.81
Ding et al. (2020)	20	Participants from ongoing normal aging study. Average age 81.2 (SD 7.15) years. 70% Females. 85% white and 15% African-Americans	T1W, FLAIR / 3T	Supervised	DSC 0.78, FPR 0.009 PPV 0.85, TPR 0.70

White Matter Hyperintensities Segmentation Review

Fiford et al. (2020)	60	30 controls and 30 AD patients from ADNI. Mean age controls 73.4 (6.2) years Mean age AD patients 74.9 years	T1W, FLAIR / 3T	Unsupervised	DSC 0.74 (F/T PR and NR given by anatomical regions)
Hong et al. (2020) https://github.com/jisu-hong/deepwmh	148	Patients with migraine without aura, migraine with typical aura, and chronic migraine. Mean age: 44.4 years, 82 Females	T1W, FLAIR / 3T	Deep learning	TPR 0.87, FDR 0.10
Liu et al. (2020)	60	Data from WMH segmentation challenge (https://wmh.isi.uu.nl/), and SISS challenge 2015. Out of 60, 25 cases contained ischemic stroke lesions	T1W, FLAIR / 1.5T & 3T	Deep learning	DSC 0.829
Rachmadi et al. (2020) https://github.com/febrianrachmadi/lots-iam-gpu	60	20 subjects from ADNI and 40 MS patients with different loads of MS lesions.	T1W, T2W, FLAIR / 3T	Unsupervised	DSC 0.47 - 0.56 PPV 0.59 TPR 0.47

Legend: ADNI: Alzheimer's Disease Neuroimaging Initiative, AD: Alzheimer's disease, MCI: Mild Cognitive Impairment, M:F (or F:M): number of Male : number of Female (or viceversa) participants, CADASIL: Cerebral autosomal dominant arteriopathy with subcortical infarcts and leuko-encephalopathy, T1W: T1-weighted MRI sequence, T2W: T2-weighted MRI sequence, FLAIR: fluid attenuated inversion recovery MRI sequence, PD: proton density MRI sequence, 1.5T/3T: MRI scanner magnet strength 1.5 or 3 Teslas, DSC: Dice Similarity Coefficient, TPR: True Positive Rate (equivalent to Recall and Sensitivity), FNR: False Negative Rate, FPR: False Positive Rate, TNR: True Negative Rate (equivalent to Specificity), PPV: Positive Predictive Value (equivalent to Precision), WMH: white matter hyperintensities, MS: Multiple Sclerosis

Risk of Bias Assessment within Studies

We observed four types of bias: spectrum bias, observer bias, verification bias and selection bias (Figure 3). Observer and data selection biases were common. Observer bias, found in 23/37 studies, mainly occurred in studies that proposed a supervised segmentation method. These "learned" from reference data generated by one or various observers or used limited overlapping retrospective data. A study that reported consensus between observers in the generation of reference segmentation data proposed an unsupervised segmentation method (Sudre et al., 2015). Data selection bias was also observed in 25/37 studies.
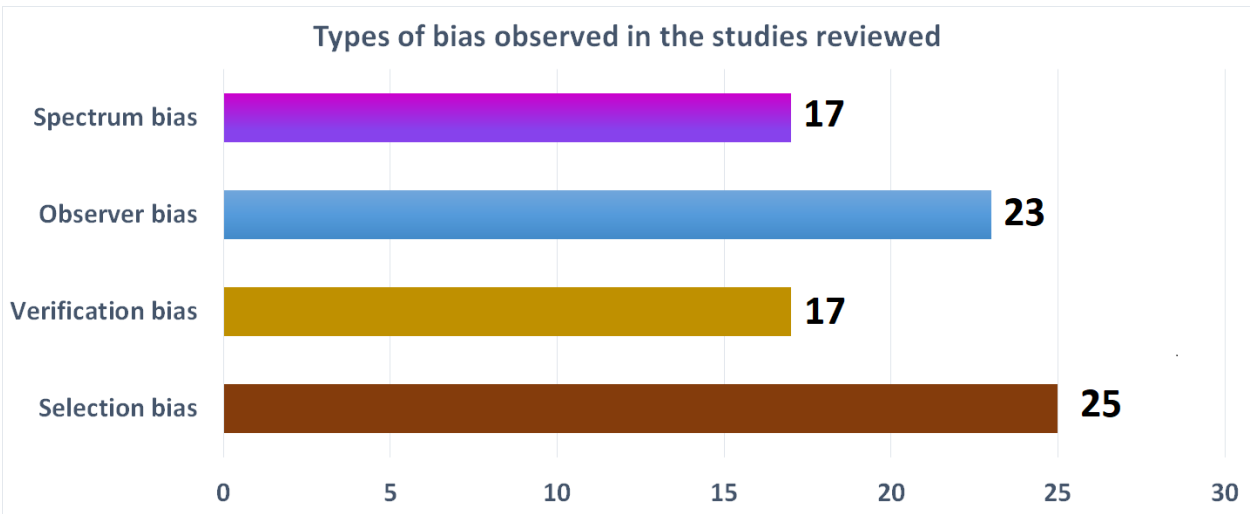
Figure 3. Types of bias observed in the articles reviewed.

Lack of considering differences in the level of disease severity (i.e. WMH burden in relation to underlying disease/population group) are referred to as spectrum bias (Schmidt et al., 2013). Eighteen studies did not clearly report clinical features and disease characteristics of individuals included in terms of WMH severity. Therefore, it was difficult to judge whether or not a wider and balanced spectrum of WMH burden was present in the sample and, consequently, if the methods were biased towards data with higher, medium or small burden of WMH in a certain population group.

Data inclusion and exclusion criteria were not explained in 22/37 studies. Of the studies that reported demographic information, five recruited healthy controls (Griffanti et al., 2016; Sundaresan et al., 2019; Damangir et al., 2017; Rincón et al., 2017; Ding et al., 2020). One study stated that the data selection and manipulation were blinded to clinical information (i.e., avoided clinical review bias) (Dadar et al., 2017a). One study reported having selected the cases randomly (Atlason et al., 2019).

The magnet strength of the scanner used to acquire the data processed was reported in 35/37 studies (see Table 2). Twelve studies used data only acquired at 1.5T, and twelve used data only

acquired at 3T. Only 11/37 studies used data acquired at both 1.5T and 3T (Atlason et al., 2019; Dadar et al., 2017a; Jiang et al., 2018; Knight et al., 2018; Li et al., 2018; Ling et al., 2018; Liu et al., 2020; Manjón et al., 2018; Sundaresan et al., 2019; Wang et al., 2015; Wu, Zhang, Wang & Tang, 2019).

We observed differential verification bias in 17 studies. These studies used different reference standards to verify segmentation method's performance; i.e., more than one reviewer was involved in manual WMH delineation of different datasets, or each dataset was delineated by a different person using different strategies, without stating degree of inter-observer reliability or whether or not the final reference segmentation was agreed between the observers involved. Only 8/37 studies made the code publicly available (Griffanti et al., 2016; Hong et al., 2020; Jiang et al., 2018; Li et al., 2018; Park et al., 2018; Rachmadi et al., 2018, 2020; Valverde et al., 2017). A study (Ling et al., 2018) evaluates different configurations of the method described by Griffanti et al. (2016) making recommendations of its use. We present risk of bias assessment of the 37 included studies using QUADAS 2 tool in Table 3. Out of the 37 studies, only 7 were judged as having low risk of bias overall.

Table 3: Risk of Bias Assessment of the studies reviewed using QUADAS 2 Tool (https://www.bristol.ac.uk/media-library/sites/quadas/migrated/documents/quadas2.pdf). Studies appear in alphabetical order of the first author's surname by year of publication.

STUDY	RISK OF BIAS						APPLICABILITY		
	PATIENT SELEC-TION	INDEX TEST	REFERENCE TEST		FLOW &TIMING		PATIENT SELEC-TION	INDEX TEST	REFE-RENCE TEST
	Could the selection of patients have introdu-ced bias?	Could the method have introdu-ced bias?	Is the ref. std. likely to be correct?	Is the ref. std. mani-pulated blind to the	Did all data had the same ref. std.?	Were all patients included ?	The included patients match the review question?	Are there concerns re. appli-cability?	Are there concerns re. reprodu-cibility?

				index test?					
Roy et al. (2015)	🙂	🙁	🙂	🙂	🙂	🙂	🙂	🙂	🙂
Sudre et al. (2015)	🙁	🙂	🙂	🙂	😐	😐	🙂	🙂	🙂
Van Opbroek et al. (2015a)	🙁	🙁	🙂	🙂	🙁	😐	🙁	🙁	🙂
Van Opbroek et al. (2015b)	🙁	🙁	🙂	🙂	🙂	😐	🙁	🙁	🙂
Wang et al. (2015)	🙁	🙂	🙂	🙂	🙂	🙂	🙁	🙂	🙂
Zhan et al. (2015)	🙁	🙂	🙂	🙂	🙂	🙂	🙁	🙂	🙁
Damangir et al. (2016)	🙂	🙂	🙂	🙂	🙂	🙂	🙁	🙂	🙂
Griffanti et al. (2016)	🙂	🙁	🙂	🙂	🙁	🙂	🙂	🙂	🙂
Stone et al. (2016)	🙂	🙁	🙂	🙂	🙂	🙁	🙂	🙂	🙂
Bowles et al. (2017)	🙁	🙂	🙁	🙂	🙁	🙁	😐	🙂	🙂
Dadar et al. (2017a)	🙂	🙁	🙂	🙂	🙂	🙂	🙂	🙂	🙂
Ghafoorian et al. (2017)	🙂	🙁	🙂	🙂	🙂	🙁	🙂	🙂	🙂
Rincón et al. (2017)	🙂	🙁	🙂	🙂	🙂	🙂	🙂	🙂	🙂
Sudre et al. (2017)	🙁	🙂	🙂	🙂	😐	🙂	😐	🙂	🙂
Valverde et al. (2017)	🙁	🙂	🙂	😐	🙁	🙂	🙁	🙂	🙁
Zhan et al. (2017)	🙂	🙁	🙂	🙂	🙂	🙂	🙂	🙂	🙂

Bandeira Diniz et al. (2018)	🔴	🔴	🔴	🟢	🟢	🟢	🔴	🟢	🟢
Guerrero et al. (2018)	🟢	🔴	🟢	🟢	🔴	🟢	🟢	🟢	🔴
Jiang et al. (2018)	🔴	🔴	🟢	🟢	🔴	🟡	🟢	🟢	🟢
Knight et al. (2018)	🔴	🔴	🟢	🟢	🔴	🟢	🔴	🟢	🟢
Li et al. (2018)	🔴	🔴	🟡	🟢	🟡	🟢	🔴	🟢	🔴
Ling et al. (2018)	🟢	🔴	🟢	🟢	🟢	🟢	🟢	🟢	🟢
Manjón et al. (2018)	🟢	🔴	🟢	🟢	🟢	🟢	🔴	🟢	🟢
Moeskops et al. (2016)	🔴	🔴	🟢	🟢	🔴	🔴	🟢	🟢	🟢
Park et al. (2018)	🟢	🔴	🟢	🟢	🔴	🔴	🟢	🟢	🟢
Qin et al. (2018)	🔴	🟢	🟢	🟢	🟡	🟢	🔴	🟢	🟢
Rachmadi et al. (2018)	🟢	🔴	🟢	🟢	🟢	🟢	🔴	🟢	🟢
Atlason et al. (2019)	🟢	🟢	🟢	🟡	🔴	🟢	🔴	🟢	🟢
Schirmer et al. (2019)	🟢	🔴	🟢	🟢	🔴	🔴	🟢	🟢	🟢
Sundaresan et al (2019)	🟢	🔴	🟡	🟡	🔴	🟢	🟢	🟢	🔴
Wu et al. (2019)	🟢	🟢	🟢	🟢	🟢	🟡	🟢	🟢	🟢
Wu, Zhang, Wang & Tang (2019)	🔴	🟢	🔴	🟡	🟢	🟢	🔴	🟢	🟢
Ding et al. (2020)	🔴	🟢	🟢	🟡	🔴	🔴	🔴	🟢	🟢
Fiford et al. (2020)	🔴	🟢	🟢	🟡	🟢	🟢	🔴	🟢	🟢

Hong et al. (2020)	🙂 Low	😐 Unclear	🙂 Low	😐 Unclear	🙂 Low	🙂 Low	🙂 Low	🙂 Low	🙂 Low
Liu et al. (2020)	☹️ High	😐 Unclear	🙂 Low	😐 Unclear	🙂 Low	😐 Unclear	☹️ High	🙂 Low	🙂 Low
Rachmadi et al. (2020)	☹️ High	🙂 Low	🙂 Low	🙂 Low	🙂 Low	🙂 Low	☹️ High	🙂 Low	🙂 Low

☹️ - High   😐 - Unclear   🙂 - Low

Pre-processing Methods

All studies which reported ground truth generation details, validated the WMH segmentation method with ground truth binary masks generated using the Fluid Attenuated Inversion Recovery (FLAIR) MRI sequence. However, only three studies reported having used only the FLAIR sequence in their segmentation framework (Bandeira Diniz et al., 2018; Knight et al., 2018; Schirmer et al., 2019). From the rest (i.e., 34/37) that described using data from different sequences, 28 used a combination of more than one sequence (i.e., also known as "multispectral approach"), generally T1-weighted and FLAIR, to generate the final outcome. In general, after MRI acquisition, various pre-processing steps were conducted. These often were registration, brain extraction, intensity inhomogeneity correction, noise reduction and intensity normalisation. Table 4 summarises the publicly available tools used in the studies' pipelines and Table 5 summarises the pre-processing steps used by each study. Only one study reported having conducted all the above-mentioned pre-processing steps prior to the segmentation method (Manjón et al., 2018), and one did not provide any information about pre-processing steps performed before segmentation (Liu et al., 2020). The latter selected MRI slices from already brain-extracted images downloaded from an image data repository without specifying how the slice selection was performed (i.e., by visual inspection or automatically). The slice selection excluded 81 slices with haemorrhagic stroke and those at the top and bottom of the brain, which are more prone to have confounding artefacts.

Table 4. Publicly available software resources and tools used in the selected studies

White Matter Hyperintensities Segmentation Review

Software library / Repository	Tool	Use	References / Documentation
FMRIB software library (FSL) https://fsl.fmrib.ox.ac.uk/fsl/fslwiki/	Brain Extraction Tool (BET)	Removal of non-brain tissues	Smith (2002); Jenkinson, Pechaud and Smith (2005)
	FMRIB's Linear Image Registration Tool (FLIRT)	Linear (affine) intra- and inter-modal brain image registration	Jenkinson and Smith (2001) Jenkinson, Banner, Brady and Smith (2002)
	FMRIB's Automated Segmentation Tool (FAST)	Tissue segmentation and correction for bias field inhomogeneities	Zhang, Brady & Smith (2001)
Statistic Parametric Mapping (SPM) https://www.fil.ion.ucl.ac.uk/spm/software/	Set of MATLAB scripts and functions integrated in a graphic interface environment that can be used independently		("SPM - Documentation", 2020)
Advanced Normalization Tools (ANTs) https://sourceforge.net/projects/advants/v, http://stnava.github.io/ANTs/, https://github.com/ANTsX/ANTs	antsRegistration	Part of the ANTs suite of image registration tools	("Advanced Normalization Tools (ANTs) - SourceForge.net", 2020) (http://stnava.github.io/ANTs/) ("ANTsX/ANTs", 2020)
	N3, N4	Correction for bias field inhomogeneities	Tustison et al. (2010)
bric1936 https://sourceforge.net/projects/bric1936/	bricBET (MATLAB wrappers to FSL-BET)	Generation of the intracranial volume binary mask from combinations of multiple MRI sequences	https://sourceforge.net/projects/bric1936/files/Documentation/
3DSlicer https://www.slicer.org/	Modules for Image registration https://www.slicer.org/wiki/Slicer3:Registration		("Documentation/4.10/Training - Slicer Wiki", 2020)
Medical Image Registration Tool (MIRTK) https://biomedia.doc.ic.ac.uk/software/mirtk/ https://github.com/BioMedIA/MIRTK	Image registration		("MIRTK – BioMedIA", 2020)
OptiBET https://montilab.psych.ucla.edu/fmri-wiki/optibet/	Brain extraction (uses FSL-BET)		Lutkenhoff et al. (2014)
Elastix https://en.freedownloadmanager.org/Windows-PC/Elastix-FREE.html https://elastix.lumc.nl/download.php	Image registration		Klein et al. (2010); Shamonin et al. (2014)
Niftyreg https://sourceforge.net/projects/niftyreg/ https://www.nitrc.org/projects/niftyreg/	Image registration		Modat et al. (2014)

MRIcro https://www.mccauslandcenter.sc.edu/crnl/mricro https://www.nitrc.org/projects/mricron/	Brain extraction and delineation of regions of interest	("MRIcro | CRNL", 2020) ("NITRC: MRIcron: Document Manager: Display Document", 2020)
Freesurfer https://surfer.nmr.mgh.harvard.edu/	Image segmentation (Anatomical segmentation of regions of interest)	("FreeSurferWiki - Free Surfer Wiki", 2020)
Multi-cONtrast brain STRipping (MONSTR) https://www.nitrc.org/projects/monstr	Brain extraction	Roy et al. (2017)
Analysis of Functional NeuroImages (AFNI) https://afni.nimh.nih.gov/	Space transformation, visualisation, and statistical analyses of fMRI data	https://afni.nimh.nih.gov/pub/dist/doc/htmldoc/index.html (Cox, 1996)

Table 5. Pre-processing in the studies involved. Studies appear in alphabetical order of the first author's surname by year of publication (as per previous tables).

STUDY	REGISTRATION (details reported)	BRAIN EXTRACTION	INTENSITY INHOMOGENEITIES CORRECTION	NOISE REDUCTION	INTENSITY NORMALISATION
Roy et al. (2015)	Rigid-body – uses SPM 8	FSL-BET	N3	Information not provided	Histogram matching (Nyul et al., 2000)
Sudre et al. (2015)	Intra-subject inter-modality co-registration, and statistical atlases warped to observed data using niftyreg	Performed using STEPS (Cardoso et al. 2013) followed by non-brain tissue mask filling	Information not provided	Information not provided	Intensity rescaling from 0 to 1.
Van Opbroek et al. (2015a)	Information not provided	Information not provided	N4	Information not provided	Three normalisation algorithms were evaluated: 1) Range-matching (maps the 4th and the 96th percentage of intensity within the brain mask to 0 and 1.

					2) Linear intensity adjustment to the range [0,1]. 3) Method 1 followed by mapping of every tenth percentile within 0 and 1 to the mean intensity over all (training and target) images
Van Opbroek et al. (2015b)	Information not provided	FSL-BET	N4	Information not provided	Range-matching procedure that scaled the voxels within a mask such that the voxels between the 4th and 96th percentage in intensity are mapped between 0 and 1
Wang et al. (2015)	Information not provided	Brain Extraction Tool in MRIcro	N3	Information not provided	Image intensity rescaling from 0 to 255
Zhan et al. (2015)	A mutual information-based registration method (Viola and Wells, 1997)	FSL-BET	N3	Information not provided	Information not provided
Damangir et al. (2016)	Intra-subject, rigid, 3-D with mutual information - uses FSL FLIRT	FSL-BET	N3	Information not provided	Information not provided
Griffanti et al. (2016)	Linear, with trilinear interpolation (in multisequence evaluation using T1-weighted and FLAIR) - uses FSL-FLIRT	Information not provided	Information not provided	Information not provided	Used variance scaling
Stone et al. (2016)	Rigid-body, linear intra-subject, of FLAIR, T1- and T2-weighted sequences – uses ANTs	ANTs	N4 bias correction	Information not provided	Normalized to the intensity range 0–1.

White Matter Hyperintensities Segmentation Review

Bowles et al. (2017)	Rigid-body, linear, of T1-weighted to FLAIR followed by free-form deformation between T1-weighted image in FLAIR image space and an MNI template –uses MIRTK suite	pincram algorithm (uses label propagation and group agreement) (Heckemann et al., 2015)	N4 algorithm	Information not provided	Linear scaling using the mean intensity of the healthy (i.e., gray and white matter) tissue in the cohort (estimated having the value of 1000). (Huppertz et al., 2011)
Dadar et al. (2017a)	Intra-subject, linear rigid body, of T2-weighted, PD and FLAIR to T1-weighted, then non-linear based on intensity correlation coefficient to ADNI 150 template	Information not provided	N3	Automatic multi-threaded denoising method based on non-local means filtering (Manjón et al. 2010)	Linear intensity scaling using histogram matching to a template from 150 subjects (50 normal controls, 50 MCI and 50 dementia) from ADNI database (i.e., ADNI150)
Ghafoorian et al. (2017)	Rigid-body, linear, of T1-weighted to FLAIR with trilinear interpolation and mutual information optimization – uses FSL-FLIRT	FSL-BET on T1-weighted images	FSL-FAST	Information not provided	Normalized per patient to be within the range of [0, 1]
Rincón et al. (2017)	Linear, intra-subject, of T1-weighted to FLAIR – uses BRAINSFit from 3D–Slicer	White matter tissue and ventricles segmented using Freesurfer	SPM 8	Information not provided	Normal white matter modelled for Gaussian fit to generate parameters for FLAIR intensity normalisation using the EzyFit Toolbox ("EzyFit 2.44", 2020)
Sudre et al. (2017)	Affine, linear, intra-subject, of FLAIR to T1-weighted. Non-linear (niftyreg) used for generating synthetic data.	Performed, but information not provided	Performed, but information not provided	Information not provided	Information not provided
Valverde et al. (2017)	Affine followed by non-linear registration of the MNI-ICBM152 brain template to the native	Information not provided	Information not provided	Information not provided	Information not provided

Balakrishnan, Valdes-Hernandez and Farrall

	T1-weighted space - used niftyreg followed by the registration tool in SPM12.				
Zhan et al. (2017)	Information not provided	FSL-BET on T1-weighted images	N3 bias field correction	Information not provided	Linear contrast adjustment to match the intensities of the training and testing datasets
Bandeira Diniz et al. (2018)	Not applicable (uses only FLAIR images)	Algorithm by Bauer et. al. (2011)	Information not provided	Information not provided	histogram matching algorithm
Guerrero et al. (2018)	T1-weighted registered to FLAIR - uses FSL-FLIRT	Information not provided	Information not provided	Information not provided	Tissue intensities normalised to have zero mean and standard deviation of one (excluding the background).
Jiang et al. (2018)	Rigid body, linear, of FLAIR to T1-weighted and from T1-weighted space to the Diffeomorphic Anatomical Registration Through Exponentiated (DARTEL) space - uses SPM 12	SPM 12 – used brain mask in DARTEL space to remove non-brain tissues	FSL-FAST	Information not provided	Information not provided
Knight et al. (2018)	Training images are resampled (trilinear) to 1.5mm isotropic voxel resolution in the MNI-ICBM152 space – uses the Segment tool in SPM 12	Segment tool in SPM 12	Segment tool in SPM 12	Information not provided	Information not provided
Li et al. (2018)	(Retrospective data, intra-subject MRI sequences previously co-registered)	(data was already brain extracted)	SPM12	Information not provided	Gaussian intensity normalisation
Ling et al. (2018)	Linear, of FLAIR to T1-weighted space and from T1-weighted to	FSL-BET	Information not provided	Information not provided	Variance scaling within FSL- BIANCA

	MNI-ICBM152 standard space				
Manjón et al. (2018)	Linear registration to the MNI-ICBM152 space – uses ANTs	SPM12	SPM12	Spatially Adaptive 3D Non-local Means Filter	All brain voxels intensities were divided by the median intensity within the brain region. Resulting intensities were squared to enhance image contrast
Moeskops et al. (2018)	Intra-subject, of T1-weighted (with and without inversion recovery pulse) to FLAIR – uses elastix (Klein et al., 2010)	SPM 12	SPM 12	Information not provided	Information not provided
Park et al. (2018)	Rigid-body – uses FSL-FLIRT	FSL-BET	FSL-FAST	Information not provided	Information not provided
Qin et al. (2018)	Rigid-body, linear, of T1-weighted and FLAIR - uses FSL-FLIRT	Information not provided	As per the unified segmentation algorithm in SPM5	Information not provided	As per the unified segmentation algorithm in SPM5
Rachmadi et al. (2018)	Rigid-body, linear - uses FSL-FLIRT	OptiBET	Information not provided	Information not provided	Histogram matching (Nyúl et al., 2000)
Atlason et al. (2019)	Rigid registration to the MNI-ICBM152 template	skull removal using MONSTR	inhomogeneity correction using N4 integrated into SegAE	Information not provided	Information not provided
Schirmer et al. (2019)	Affine – uses ANTs	(Neuron-BE) that used a 2D U-Net convolutional neural network architecture	Information not provided	Information not provided	Mean-shift algorithm and corresponding full width half maximum (FWHM) of the peak in the intensity histogram of the total brain volume

Sundaresan et al. (2019)	Rigid-body, linear – uses FSL FLIRT	FSL-BET	FSL-FAST	Information not provided	Information not provided
Wu et al. (2019)	FLAIR to T1-weighted previously mapped in MNI-ICBM152 coordinates - uses SPM (version not specified)	Information not provided	N4 bias correction	Information not provided	Histogram matching
Wu, Zhang, Wang & Tang (2019)	Information not provided (Retrospective data, intra-subject MRI sequences previously co-registered)	FSL-BET	Information not provided	Information not provided	Gaussian intensity normalization (z-scores)
Ding et al. (2020)	Linear within-subject co-registration of FLAIR and T!W sequences using FSL-FLIRT through fslr (Muschelli et al., 2018)	FSL-BET followed by erosion of the brain mask through fslr (Muschelli et al., 2018)	N4	Information not provided	z-scores calculated over the entire brain-only intensity signal
Fiford et al 2020	Information not provided	skull-stripped and atlases obtained from label fusion GIF framework (Cardoso et al. 2015).	Method proposed by Van Leemput et al (1999)	Information not provided	Information not provided
Hong et al. (2020)	Rigid-body linear within-subject co-registration of T1W and FLAIR sequences	Information not provided	Information not provided	Information not provided	Information not provided
Liu et al. (2020)	Information not provided	Information not provided	Information not provided	Information not provided	Information not provided
Rachmadi et al. (2020)	Rigid-body linear within-subject co-registration of T1W and FLAIR sequences using FSL-FLIRT	OptiBET and bricBET (applied to separate datasets)	Information not provided	Information not provided	Information not provided

Legend: T1W: T1-weighted structural magnetic resonance (MRI) sequence, FLAIR: fluid-attenuated inversion recovery structural MRI sequence, MNI-ICBM152 template: Montreal Neurological Institute –

White Matter Hyperintensities Segmentation Review

International Consortia for Brain Mapping brain template from 152 healthy young adults that includes both a set of coordinates and the associated anatomical labels,
Note: for list of software tools, please, refer to Table 4.

Most studies included in the review used linear transformation models to co-register the different image sequences from each subject data (Figure 4 (left hand side), Table 5). From the 27/37 studies that provided information on the tool used for image registration, ten used FSL FLIRT (Qin et al., 2018; Griffanti et al., 2016; Guerrero et al., 2017; Sundaresan et al., 2019; Damangir et al., 2017; Rachmadi et al., 2018, 2020; Ghafoorian et al., 2017; Hong et al., 2020; Ding et al., 2020), three used ANTs (Schirmer et al., 2019; Manjón et al., 2018; Stone et al., 2016), five used SPM (Wu et al., 2019; Roy et al., 2015; Jiang et al., 2018; Knight et al., 2018; Valverde et al., 2017), one study used elastix (Moskops et al., 2018), one study used 3DSlicer (Rincon et al., 2017), and one study used MIRTK (Bowles et al., 2017). The skull stripping method for removal of non-brain tissues was reported in 25/37 studies: FSL-BET, ANTs, OptiBET, Neuron BE, SPM, Freesurfer, MONSTR and MRIcro. Intensity inhomogeneity correction was reported in 17/37 studies, and it was always performed using a well-known tool: N3 (or N4), SPM, FSL-FAST or the Nu estimate. N3 and its newer version N4, were the tools most commonly used for intensity inhomogeneity correction (Stone et al., 2016; Wu et al., 2019; Bowles, et al., 2017; Dadar et al., 2017a; Van Opbroek, Ikram, Vernooij & de Bruijne, 2015a, 2015b; Damangir et al., 2017; Roy et al., 2015; Wang et al., 2015; Zhan et al., 2015; Zhan et al., 2017; Atlason et al., 2019; Ding et al., 2020). Non-local means was the only filtering technique used by the two studies that reported having included noise removal within their pre-processing steps (Manjón et al., 2018; Dadar et al., 2017a). Neither of these two studies selectively applied the filtering after analysing the signal. The 23/37 studies that provided information on intensity normalisation, reported the use of either variance / linear scaling or histogram matching, with variations in their implementation.

Segmentation Methods

From the studies included, 73% (i.e., 27/37) proposed a supervised segmentation method. Of them, 37% (i.e. 10/27) used deep learning. From the 10 studies that proposed an unsupervised segmentation method (i.e., 27% of the total number of studies included), one used deep learning (Atlason et al., 2019). In total, eleven studies used Convolutional Neural Networks (Rachmadi, et al., 2018; Li et al., 2018; Guerrero et al., 2017; Moeskops et al., 2018; Ghafoorian et al., 2016; Hong et al., 2020; Manjón et al., 2018; Wu et al., 2019; Liu et al., 2020; Diniz et al., 2018; Schirmer et al., 2019), four studies proposed a method based on k-nearest neighbours (k-NN) (Sundaresan et al., 2019; Jiang et al., 2018; Ling et al., 2018; Griffanti et al., 2016), four studies proposed regression models (Knight et al., 2018; Dadar et al., 2017a; Zhan et al., 2017; Ding et al., 2020), and three studies used Random forest (RF) in their proposed algorithms (Stone et al., 2016; Park et al., 2018; Roy et al., 2015). Two studies proposed a method based on Fuzzy C mean algorithm (Zhan et al., 2015; Valverde et al., 2017) and three proposed improvements to a Gaussian Mixture Model framework (Sudre et al., 2015, 2017; Fiford et al., 2020), both unsupervised methods. We summarize the segmentation methods included in the reviewed studies in Figure 4 (right hand side).
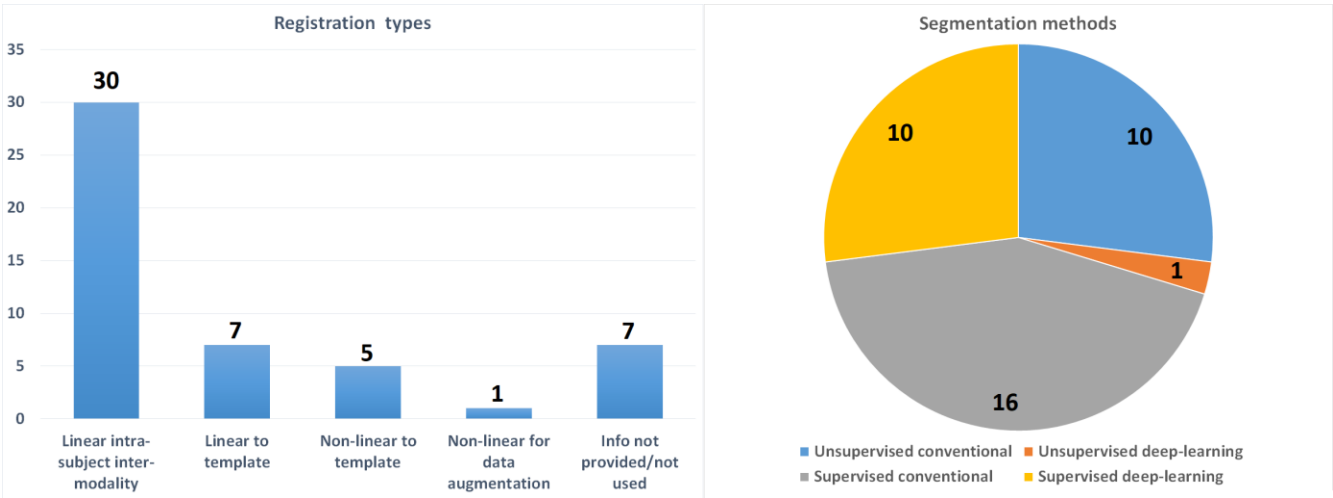
Figure 4. Co-registration procedures involved in the WMH segmentation frameworks (left) and types of WMH segmentation methods covered (right) by the articles reviewed.

Supervised WMH segmentation methods

k-Nearest Neighbours (k-NN)

k-NN is a well-established pattern recognition method that, for WMH segmentation, compares each voxel's spatial (i.e., location) and intensity features with those extracted from a training set, and assigns a probability of being (or not) WMH based on the result. This algorithm was first proposed for this task in 2000 (Warfield, Kaus, Jolesz & Kikinis, 2000), further evaluated in 2004 (Anbeek et al., 2004) and improved by additionally using spatial tissue type priors in further works (De Boer et al., 2007; Steenwijk et al., 2013). Three of the four papers included in this review that use this method (Ling et al., 2018; Griffanti et al., 2016; Sundaresan et al., 2019) use the implementation Brain Intensity Abnormality Classification Algorithm (BIANCA) of the FMRIB Software Library (FSL). BIANCA (Griffanti et al., 2016) is a versatile, easy to use, freely available implementation that offers different options for input modalities (i.e., only FLAIR or multi-sequence), weighting the spatial information, local spatial intensity averaging, and for the choice of the number and location of the training points. Ling et al. (2018) evaluated BIANCA using: 1) input modalities FLAIR alone vs FLAIR and T1-weighted; 2) applying different thresholds to BIANCA's probabilistic output, and highlighted the high number of false positives observed when using the FLAIR sequence alone compared to those obtained when the multispectral approach is used. Sundaresan et al. (2019) improved BIANCA to accommodate variability of sources and automatically optimise the thresholding of the lesion probability map by adaptively determining local thresholds, instead of adopting a global threshold. For this purpose (i.e., calculating and generating the local thresholds), the study presents the Locally Adaptive Threshold Estimation (LOCATE) algorithm.

Jiang et al. (2018) incorporate WMH cluster size as a third feature in the k-NN algorithm, and integrate it in a pipeline called UBO detector, freely available from https://cheba.unsw.edu.au/research-groups/neuroimaging/pipeline. UBO detector merges registration and normal tissue segmentation functions available in two different software libraries (i.e., SPM the FMRIB Software Library) for pre-processing and uses T1-weighted and

FLAIR images as input. Although UBO uses a supervised algorithm for WMH segmentation, can prescind from manual generated labels for training by taking candidate clusters from the priors generated in the pre-processing stage. As the authors recognise, the accuracy in segmenting WMH depends on the accuracy of the segmentation of candidate WMH clusters obtained from FSL-FAST.

Large Margin Classifiers

Large margin algorithms maximise the margin around the decision boundary of a classifier to reduce the uncertainty in the classification, handling well, high-dimensional data (Wu et al., 2013). Qin et al. (2018) developed a supervised large margin algorithm (SLM) followed by a semi-supervised large margin algorithm (SSLM) in a framework that modifies a self-guided labelling procedure, namely unsupervised one-class learning (UOCL) (Liu et al., 2014) , which discovers potential "outliers" in the data, being these the WMH. Qin et al. (2018) introduced a new term in the objective function of the UOCL that maximises the average margin between the hyperintensities (i.e. considered outliers) and the decision boundary. The general SLM classifier minimises the objective function using a conjugate gradient method to learn from the training set and provides a rough WMH segmentation map. The SSLM, then, refines the given labels on the target data.

Multi-Atlas Segmentation

Wu et al. (2019) presented a framework that simultaneously segments the brain and detects WMH. The proposed multi atlas-based detection and localization (MADL) framework uses a multi-atlas likelihood fusion approach to segment the brain tissues and structures, and identify WMH. It uses a multi-atlas library generated from 15 FLAIR images with minimal WMH load and atrophy ranging from minimal to moderate. The Bayes maximum a posteriori estimation generates a maximum posterior probability value for each voxel, of belonging to a certain (atlas) label. The WMH are identified as voxels with maximum posterior probability values below certain threshold empirically determined.

Feature Filters

Rincón et al. (2017) present an object-based segmentation framework, namely amorphous object segmentation in 2D (AMOS -2D). This method uses a multi-level information approach consisting of a hierarchical multi-threshold WMH segmentation followed by an object-based filter that reduces the number of false-positives. After pre-processing T1-weighted and FLAIR images, AMOS-2D applies white-matter Gaussian modelling to determine the intensity distribution of the WMH. An initial WMH mask is generated using multi-threshold segmentation, which combines single grey-scale thresholding with a seed-based thresholding. In the latter, the higher threshold (i.e. seed) acts as WMH detector and the lower threshold (i.e. region) refines the contours. The optimum thresholds are determined ad-hoc from the training dataset. The filter that refines the "initial" WMH mask is an object-based classifier that uses support vector machine (SVM). The feature vector for this classifier initially consisted of 178 features, including normalised intensity, others derived from applying connected-component analysis, distance to white matter contour, distance to white matter skeleton, distance to ventricles, among others not specified. The dimensionality of the initial feature vector was reduced using correlation-based feature selection.

Roy et al. (2015) present two filtering approaches: one for generating probabilistic regions of interest (i.e. weighted candidate voxels) for the segmentation algorithm to operate, and another to post-process the classifier's output. The first are contrast-based global probabilistic maps generated from a feature set containing enhanced intensity, anatomical and spatial information, and the second is an edge potential function based Markov Random Field model, which is used to remove false positives and obtain the final output.

Regression models

Dadar et al. (2017a) proposed a multispectral linear regression classifier that uses the least-squares parameters estimation to segment WMH. It combines intensity and location features from FLAIR, T1-, T2- and PD-weighted MRI and manually labelled training data, to provide a

continuous subject-specific WMH map displaying different levels of tissue damage along with a binary segmentation.

Knight et al. (2018) developed a supervised logistic regression framework exclusively for FLAIR sequences, called Voxel-Wise Logistic Regression. This method modifies the open source Lesion Segmentation Tool (LST) LPA by estimating the voxel-wise logistic regression parameters simultaneously across the image space for facilitating convergence during the parameters' estimation, instead of randomly sampling the image space. The logistic model, trained using the standardised FLAIR intensity levels of a training set, generates a set of parameters that are subsequently smoothed for their use in the lesion prediction for new images.

Zhan et al. (2017) developed a supervised method that integrated the multi-sequence and spatial information in a Bayesian framework for WM lesion detection from multi sequence MR images. The proposed method is based on a three-step approach: 1) multinomial logistic regression is employed to learn the conditional probability distributions of WMH and brain tissues from training data; 2) spatial information from Markov random field priors is merged with multi sequence information in the Bayesian framework to improve the accuracy of WMH segmentation; and 3) pathology background information is used to reduce false positives.

Ding et al. (2019) present a supervised segmentation method called OASIS-AD. This approach is derived from a previous scheme (i.e., OASIS, Sweeney et al., 2013) developed for MS lesion segmentation, which uses a logistic regression model involving several imaging modalities to determine the probability of a voxel being WMH or not. This model uses as input brain-extracted and normalised image data. The enhanced version OASIS-AD additionally erodes the brain-extracted binary mask generated in the pre-processing step and refines the probability map obtained from the regression model by applying a nearest neighbour feature construction approach that uses FSL-FAST (Zhang, Brady & Smith, 2001), followed by a Gaussian filter.

Random Forest (RF)

Park et al. (2018) present a machine learning based pipeline called DEWS (DEep White–matter hyperintensity Segmentation framework). The authors segment the normal appearing white matter using FSL-FAST and use a combination of morphological operations and multi-level thresholding and inter-sequence registration to generate a normal white matter space that contained only deep WMH clusters in the FLAIR space. Then, a RF classifier uses size, texture and multi-parametric intensity statistical parameters from deep WMH (from a training set) as features for detecting small, superficially located deep WMH.

Stone et al. (2016) propose a multispectral framework that concatenates two RF classifiers, which the authors refer as a "two-stages" scheme. The first stage uses image intensity, symmetry, tissue segmentation voxel-wise probabilities, distance maps and neighbourhood statistics from the training data as features. These are used to produce the voxel-wise 'voting maps' (i.e. the classification count of each decision tree for each tissue label) of the first RF classifier for their use as tissue priors in a second multispectral 6-tissue segmentation that additionally uses a Markov Random Field as spatial prior. The second stage uses all Stage 1 features plus the Stage 1 voting maps and the resulting posterior probability images as features for the second RF classifier. The whole framework is constructed on Advanced Normalization Tools (ANTs) and ANTsR toolkits. Stone et al. (2016) suggested that proposed supervised method is suitable for large dataset. However, this method is tested in a small sample size.

Roy et al. (2015) use a set of nine features as input to the RF classifier. The first eight features contain multi-sequence (i.e. from T1-weighted and FLAIR) intensity, anatomical and spatial information per voxel. These are generated from probability maps of cerebrospinal fluid, grey and white matter, and normalised (x,y,z) coordinates in the MNI 152 space. The last feature is the global reference points-based contrast resulted from the filtering technique referred previously.

Support Vector Machine (SVM)

Van Opbroek et al. (2015a,b) evaluate different transfer-learning approaches in linear and non-linear SVM classifiers, all consisting of different strategies for weighting the feature vector. Both studies use data from different datasets acquired under different scanning protocols and conclude that their transfer learning strategy (i.e. weighting the feature vector) outperforms the conventional SVM using non-weighted features. In Van Opbroek et al. (2015a) authors evaluate two feature sets: one of size 6 and other of size 33. The former uses the intensity and x,y,z voxel coordinates of cerebrospinal fluid, white and grey matter probabilistic segmentations in FLAIR and the latter uses the same features but also for T1- and T2/PD-weighted, using Gaussian kernels of σ = 0.5, 1 and 2 mm^3. In Van Opbroek et al. (2015b), the authors add the gradient magnitude and the Laplacian of the normalized intensities after convolution with the Gaussian kernel at different scales and recommend using always a feature vector higher than 10 in size.

Van Opbroek et al. (2015a) assign weights to each feature of the feature vector in a way that the sum of all weights equals the total number of training samples, and combine training data with the same intensity distribution with data with different distribution in three weighting schemes: 1) Weighted SVM; 2) Re-weighted SVM; and 3) TransAdaBoost. In (1) lower weights are assigned to misclassified training data with different distribution. In (2) the misclassified lower weights (i.e. from (1)) are iteratively reduced. TransAdaBoost increases the weights of misclassified same-distribution data and reduces those from misclassified different-distribution data, but this scheme was the worst performer. In the same study authors also evaluate the namely "Adaptive SVM" that uses a weighted vector from same-distribution data for training and is tested from different-distribution data.

Van Opbroek et al.(2015b) rather evaluates three different point distribution functions (PDFs) dissimilarity measures to generate the optimal weights for the Weighted SVM classifier – the winner scheme from those evaluated in (2015a)-, which in this case uses a Gaussian kernel. The weights are chosen in an unsupervised manner, by minimizing the difference between the PDFs

of the weighted training images and the PDF of the target image. The three PDF dissimilarity measures evaluated are: 1) the Kullback–Leibler divergence; 2) the Bhattacharyya distance; and 3) the squared Euclidean distance. The optimal weights are determined by minimizing these three dissimilarity criteria while constraining them to the range [0;1] and that the norm of all the weights should be 1, using the interior-reflective Newton method (Coleman and Li, 1996).

Neural Networks

Moeskops et al. (2018) evaluated the 3-pathway multi-scale (i.e. patch-wise) convolutional neural network (CNN) scheme developed by the same group in 2016 for segmenting normal tissues in neonatal and young adults (Moeskops et al., 2016) to segment WMH in addition to normal tissues in MRI scans for older individuals / patients. In this occasion, the scheme uses the T1-weighted, T2-weighted, FLAIR and T1-weighted inversion recovery (IR) images as input. Along with WMH, the scheme segmented normal-appearing white matter, cortical grey matter, basal ganglia, thalamus, cerebellum, brain stem, lateral ventricular cerebrospinal fluid, and peripheral cerebrospinal fluid.

Bandeira Diniz et al. (2018) use Simple Linear Iterative Clustering (SLIC) to group pixels based in their location and intensities and generate candidates to lesion / non-lesion regions in each FLAIR axial slice. Authors design a single-pathway CNN for extracting implicit features from the "superpixels" of the FLAIR axial slices presented as input and classify them in lesion regions or non-lesion regions. The CNN seems to have a linear deep architecture, developed ad-hoc for this purpose. This approach resulted efficient in heterogeneously sourced data, reporting a negligible number of false positives.

Rachmadi et al. (2018) proposed an adaptation of a dual-pathway CNN scheme developed for segmenting brain lesions with considerable mass effect (Kamnitsas et al., 2017) to segment WMH. The authors introduced a way to integrate spatial information to the CNN scheme for WMH segmentation called global spatial information (GSI), and evaluate the performance of two configurations (i.e. with 8 and 5 convolutional layers) using only FLAIR vs. using a

combination of T1-weighted and FLAIR, and repeated the experiments using a single-pathway CNN architecture with and without GSI. Authors recommend the use of GSI in a multispectral (i.e. using more than one MRI sequence) dual-pathway scheme of the 2D CNN architecture evaluated.

Manjón et al. (2018) present an ensemble of patch-wise neural network classifiers for segmenting WMH on FLAIR images. After a lesion candidate ROI selection, a feature vector containing 58 features (voxel intensities from 3x3x3 and 5x5x5 patches, 3 spatial coordinates and one *a priori* lesion probability) is used by an ensemble of two one-hidden layer feedforward multilayer perceptron which performs the classification. The study evaluates two ways of configuring this ensemble: bagging (Bootstrap aggregating) and boosting. The first approach averages the outputs of the two neural network classifiers, independently trained on different randomly selected datasets. The second approach uses the output from one classifier to improve the next one by either iteratively giving more weight in the next classifier, to the samples wrongly classified in the first one, or non-randomly selecting (i.e. on the training dataset) with higher probability samples wrongly classified previously.

Guerrero et al. (2018) use the UResNet CNN architecture to segment WMH and distinguish them from stroke lesions. This method comprised an analysis path that gradually learned low- and high-level features, followed by a synthesis path, that gradually combined and up samples the low and high-level features into a class likelihood semantic segmentation. The authors confirmed that the CNN architecture performed well compared to other state of the art algorithms.

Li et al. (2018) propose a method using a 19-layer deep fully CNN scheme. In this method, WMH detected based on convolution-deconvolution architecture with long-range connections which simultaneously classified each pixel and locates objects of an input image. The scheme used ensemble models with random parameter initializations and shuffled data for voting the pixel labels in the final evaluation, all which conferred good adaptability on multi-scanners and

protocols and helped reduce overfitting. The authors pointed out that FLAIR and T1 sequences provide complementary information to detect WMH.

Schirmer et al. (2019) incorporate a deep learning CNN previously proposed by Dalca et al. in 2014, in a pipeline consisting of: 1) brain extraction using only clinical FLAIR images; 2) intensity normalisation to accommodate for multi-site heterogeneity; and 3) automatic atlas based segmentation of WMH.

Ghafoorian et al. (2016) implement several deep CNN architectures which considered multi-scale patches or explicit location features while training, to integrate the anatomical location information into the network. The authors point out that the CNNs which incorporated location information significantly outperformed a conventional segmentation method with hand-crafted features and CNNs that did not integrate location information.

Wu, Zhang, Wang & Tang (2019) modified the U-Net CNN architecture by skipping connections between the down- and up-sampling convolutional branches of the original model, and named their model Skip Connection U-Net (i.e., SC U-Net). SC U-Net additionally connects the outputs of the 4th, 7th, 10th and 13th layers in the down-sampling convolutional branch of the original model to the outputs of the 15th, 18th, 21th and 24th layers in the up-sampling convolutional branch, and feeds them (i.e., the outputs of the 4th, 7th, 10th and 13th layers) to the 16th, 19th, 22th and 25th layers. Hence the resultant model consists of a shrinking part which aims to capture context, a symmetric expansive part that gradually combines features to enable a precise localization, and a skip connection part that alleviates the vanishing gradient problem and improves the speed of the optimization convergence facilitating the training.

Liu et al. (2020) present a multi-scale feature-based CNN model, called M2DCNN not only to segment WMH, but also to distinguish them from ischemic stroke lesions. M2DCNN contains two symmetric U-shaped subnets that produce multi-scale features through the inclusion of dense and dilated blocks. The former helps reducing the number of training parameters and alleviate the gradient vanishing problem. The latter helps enlarging the receptive fields of the

convolution blocks without reducing the feature map size. M2DCNN uses a loss function based on the Dice coefficient.

Hong et al. (2020) present a deep-learning architecture that concatenates two U-Net CNN models that use 3x3 kernels in their convolutional layers. The first U-Net consists of four down-sampling and four up-sampling convolutional layers, and generates WMH priors from brain-extracted co-registered T1W and FLAIR images. These WMH candidates, together with the brain-extracted co-registered T1W and FLAIR images, are input to the second U-Net, consisting of two down-sampling and two up-sampling convolutional layers, which reduces the false-positives.

Unsupervised WMH Segmentation Methods

Damangir et al. (2017) developed an unsupervised method that statistically defined WMH based on the one-tailed Kolmogorov-Smirnov test (Gail et al., 1976).

Zhan et al. (2015) present an unsupervised WMH segmentation method for T1 and FLAIR data. The T1 image is, first, segmented into different normal tissues, among which regions of white matter and grey matter are combined to provide a region of interest that is subsequently mapped to the FLAIR image. Secondly, the authors calculated the z-score of the intensities in the ROI and defined a threshold to find the abnormalities in normal tissues. They then employ a level set method to improve the preliminary thresholding-based segmentation results and extracted the WMH. The authors pointed out that LGDF energy aided to obtain precise segmentation results compared to other level set methods that used global intensity information.

Bowles et al. (2017) propose a method built upon previous work by the same authors, which can detect abnormally hyperintense regions on FLAIR, disregarding the underlying pathology or location by combining image synthesis, Gaussian mixture models and one-class support vector machines trained only on healthy tissue.

Valverde et al. (2017) integrate a partial-volume tissue segmentation with WM outlier rejection and filling, combining intensity, probabilistic and morphological prior maps in a pipeline consisting of five steps. These are: 1) Register three statistical a-priori tissue atlases (CSF, GM and WM) and a brain structure atlas to the patient space; 2) Perform atlas-based 5-tissue segmentation on the T1-weighted image; 3) Detect and refill WM outliers as normal-appearing WM based on the registered a-priori and hyper-intense FLAIR maps if available (using the segmentation from step 2); 4) Re-estimate (again) the 5-tissue classes; and 5) Reassign intermediate volume maps into CSF, GM and WM using both neighbour and spatial prior information.

Wang et al. (2015) model the WMH in FLAIR images as having either Gumbel or Fréchet histogram distributions (see Table 1) and compare the results of their algorithm with those from applying a trimmed likelihood estimator. Although results were not accurate for all degrees of lesion loads authors recommend the principle, especially using the Fréchet distribution, due to its simplicity, for studies of ageing and vascular dementia, likely to include subjects with moderate-to-high lesion load.

Atlason et al. (2019) present an autoencoder Segmentation Auto-Encoder (SegAE) consisting on a CNN with architecture similar to that of U-Net with an additional linear layer and parameter constraints to perform linear unmixing. In this model, down- and up-sampling are performed with strided convolutions of 3D kernels of size 2x2x2 and skip connections are added between activations of the same spatial resolution from the down-sampling to the up-sampling paths. The pure tissue, WMH and cerebrospinal fluid masks obtained during the segmentation were used as priors for the N4 algorithm. Thus, the b1 inhomogeneities are corrected during the training phase and segmentation takes place in presence of inhomogeneity artifacts.

Rachmadi et al. (2020) present an unsupervised segmentation method called Limited One-Time Sampling Irregularity Map (LOTS-IM). This method generates an irregularity map (IM) that represents all voxels as irregularity values ranging from 0 to 1 with respect to the ones considered "normal" based on the original FLAIR texture information. The scheme hierarchically

samples a limited number of target squared patches (i.e., 2D patches of 1x1, 2x2, 3x3 and 4x4) from a non-overlapping grid of source patches of the same size on each brain-extracted FLAIR image slice, assigning an irregularity value to each source patch. The final irregularity map is generated by blending the hierarchically generated irregularity maps, penalizing the result using the original FLAIR intensities, and normalizing the final values between 0 and 1. The WMH are obtained by thresholding the irregularity map.

Fiford et al. (2020) examined an unsupervised segmentation method Bayesian Model Selection (BaMoS) (Sudre et al., 2015), which models the data as a multivariate mixture of Gaussians, further optimized using the expectation-maximization algorithm. It uses an initial outlier map derived after convergence of the initial Gaussian mixture model to enhance sensitivity, as proposed by Sudre et al. (2017). Newly, this study incorporates a two-threshold selection of the candidate regions and selects the WMH clusters after applying connected component analyses twice, considering first 18 neighbourhoods, and then 6 neighbourhoods, to avoid discarding regions where artefacts and true WMH are present.

Additional Publications Evaluating WMH Segmentation Methods

Dadar et al. (2017b) compare the performance of 10 different linear and non-linear supervised classification methods segmenting WMH in brain scans from 201 subjects from four different datasets. The methods evaluated are: Naïve Bayes, Logistic Regression, Linear and Quadratic Discriminant Analyses, k-NN, decision trees, RF, AdaBoost, SVM and Bagging. Out of these methods, RF was the best performer.

Kuijf et al. (2019) comparatively evaluate 20 methods presented at the 20th International Conference on Medical Image Computing and Computer Assisted Intervention (MICCAI) WMH segmentation challenge in 2019. All algorithms are trained with 60 image datasets acquired in 3 different MR scanners, and evaluated on 110 image datasets from 5 MR scanners. All image data are composed of T1-weighted and FLAIR brain-extracted, bias-corrected and co-registered

images from patients with various degrees of age-related neurodegeneration and presenting different vascular pathologies. However, the WMH volume distribution across the dataset is skewed towards low-to-medium WMH burden. From the 20 methods evaluated 14 are neural network approaches, four involve RF, one uses logistic regression, and one a three-level Gaussian mixture model. The evaluation combines the results from five similarity metrics: DSC, a modified Hausdorff distance (95th percentile), absolute percentage volume difference, sensitivity (recall), and F1-score for individual lesions. The top-ranked methods use ensembles of neural networks

Rachmadi et al. (2017) compare the performance of two conventional machine learning classifiers (i.e. support vector machine (SVM) and RF) with the performance of three deep learning algorithms, namely the deep Boltzmann machine, convolutional encoder network and a CNN dual-pathway architecture developed specifically for brain lesion detection, for segmenting WMH on brains displaying only mild or no vascular pathology. The results from these five supervised machine-learning methods are also compared with the results from the unsupervised lesion growth algorithm (LGA) of the Lesion Segmentation Tool (LST) publicly available. The evaluation uses FLAIR and T1-weighted images from 20 subjects randomly selected from the ADNI database (http://adni.loni.usc.edu/), acquired in three consecutive years, and for which ground truth WMH segmentations from two different analysts were available. Authors adapted (and/or implemented) configurations that were reported to give the highest WMH segmentation accuracy in previous works. For SVM and RF this study evaluates several combinations of feature vectors with lengths ranging from 44 to 4000, all reported previously having generated results from similar quality. The optimum threshold that defines the boundaries of the probabilistic WMH segmentations differed across methods. Differences in methods' performance depending on the WMH burden prompted authors to conclude that deep-learning methods, in general, performed better than the two conventional machine learning classifiers (i.e. SVM and RF), being the patch-based CNN configuration the best approach only for scans with low burden of WMH.

Segmentation Descriptive Quality

The descriptive quality of the segmentation methods included in the review was analyzed using the scale developed by Byrne et al. (2016). The segmentation descriptive quality (SDQ) is rated on a three point scale: 1 - indicates description of the segmentation method; 2 - indicates explanation of the segmentation method, but no description of how each step is applied; 3 – indicates full explanation of how the segmentation method proposed is applied. Out of 37, 23 studies scored 3 on this SDQ scale.

Processing Time of Segmentation Methods

Processing time of machine learning based segmentation methods refers to: 1) time taken to load the image 2) time taken for application of automatic segmentation algorithm (Cruz et al., 2017). Only 9/37 studies reported the processing time of segmentation method (Ling et al., 2018; Rachmadi et al., 2018, 2020; Manjón et al., 2018; Dadar et al., 2017a; Jiang et al., 2018; Qin et al., 2018; Griffanti et al., 2016; Atlason et al., 2019). Out of these nine studies, four reported the time consumed by the segmentation per image. It ranged from 0.03 seconds to 9 seconds per MRI. The method proposed by Qin et al. (2018) consumed considerably less time (i.e., 0.03 seconds per image) compared to the rest.

Methods evaluation

The proposed method was cross validated with leave one subject out evaluation in six studies (Stone et al., 2016; Moskops et al., 2018; Jiang et al., 2018; Knight et al., 2018; Li et al., 2018; Wu et al., 2019). Fourteen studies described a method for false positive removal (Sudre et al., 2017; Manjón et al., 2018; Stone et al., 2016; Moskops et al.. 2018; Rincón et al., 2017; Bowles et al., 2017; Li et al., 2018; Ghafoorian et al., 2017; Roy et al., 2015; Zhan et al., 2017; Hong et

al., 2020; Fiford et al., 2020; Rachmadi et al., 2020; Ding et al., 2020). Fazekas visual rating scale was used in the validation of the results in nine studies (Rachmadi et al., 2018; Qin et al., 2018; Guerrero et al., 2017; Griffanti et al., 2016; Ling et al., 2018; Moskops et al., 2018; Jiang et al., 2018; Bowles et al., 2017; Rachmadi et al., 2020).

Of the 37 studies, 30 studies evaluated the performance of the proposed segmentation method using the Dice Similarity Coefficient (DSC) among other metrics that measure spatial concordance between the results of the method proposed and reference segmentations. Average DSC values ranged from 0.538 to 0.93 (Table 2). The deep learning segmentation method proposed by Schirmer et al. (2019) reported the highest average DSC value, followed by the unsupervised schemes proposed by Damangir et al. (2016) (DSC ranging from 0.85 up to 0.91) and Wang et al. (2015) (DSC ranging from 0.81 to 0.84), and the k-NN scheme proposed by Jiang et al. (2018) (UBO detector, DSC 0.85). The Bland Altman plot (Bland & Altman, 1986) was used in five studies to analyse the volumetric agreement between the method's result and manual segmentation (Qin et al., 2018; Guerrero et al., 2017; Ling et al., 2018; Sudre et al., 2015; Fiford et al., 2020). Only four studies validated their method in longitudinal samples (Sudre et al., 2017; Jiang et al., 2018; Rachmadi et al., 2018, 2020), and eight performed an additional validation (i.e., to the traditional comparison against reference standard measurements) using clinical parameters (Guerrero et al., 2018, Jiang et al., 2018; Qin et al., 2018; Rachmadi et al., 2018, 2020; Schirmer et al., 2019; Wu et al., 2019; Fiford et al., 2020). Comparison with other methods' performance was done in 29/37 studies. The reference algorithms for excellence were the Lesion Growth Algorithm (LGA) and the Lesion Prediction Algorithm (LPA), both unsupervised methods from the Lesion Segmentation Tool (LST) for SPM (https://www.applied-statistics.de/lst.html).

DISCUSSION

In the period evaluated, 37 studies proposed new or adapted and re-purposed existing approaches for segmenting WMH of presumed vascular origin from brain MRI. Of these, only 10 were unsupervised. Within the last two years, considerable efforts have been put in developing deep learning WMH segmentation methods particularly based on CNN architectures that have demonstrated success in similar tasks. From the supervised algorithms, 37% used state-of-the-art CNN and the rest used either conventional machine-learning algorithms, the k-NN algorithm or logistic regression models. Despite the high accuracy usually reported by CNN algorithms, those reviewed do not outperform, in terms of spatial agreement with reference segmentations, the more traditional clustering (i.e. k-NN) and logistic regression supervised methods or the unsupervised methods published in this period. Probably the simplicity and strong priors of the k-NN and logistic regression methods make them easier to train with less data and less susceptible to overfitting when training data is limited compared to the deep-learning schemes. The fact that most of these methods give probabilistic outputs may be helpful in quantifying marginally pathological tissues like dirty-appearing white matter, and help in the characterisation of ill-defined WMH boundaries. However, it also conspires against their evaluation since these probabilistic results need to be binarised for comparison with manually-derived segmentation binary masks. Quality of reporting has a considerable effect on studies' value. Poor reporting of the pre-processing and segmentation methods' steps and lack of availability of the code significantly affects the applicability of various studies included in this review.

We evaluated the validity and accuracy of the segmentation methods reviewed. We refer to validity as the extent to which these algorithms measure what they intended to beyond the data used to develop (i.e., train) and validate them, thus including the applicability to other data. Most studies ignore the issues pertaining to validity and focus only on accuracy of their algorithms. The validity of the proposed segmentation methods was not always clear, mainly due to the different sources of bias in the reference used to evaluate the algorithms (i.e. observer bias in manually-delineated ground truth), the sample selection, and the data source

(i.e. mainly from a single protocol and / or acquired from scanners with the same field strength). Many studies exhibited observer bias, either in training or in evaluating their algorithms, as manual outlines of WMH are always affected by the observer's perception in recognising a true lesion from an artefact and are influenced by the observer's experience and ability in delineating the lesion boundaries on MR images. Moreover, reference segmentations are generally obtained by manually refining a semi-automatic segmentation result, obtained generally by thresholding followed by a region-growing algorithm. Selecting the optimum threshold to segment WMH from FLAIR MRI can also be a source of bias (Valdés Hernández et al., 2010). Additionally, not all the studies included were absent of having data selection bias, which can facilitate overfitting if this is not properly addressed. Data augmentation helps reducing overfitting and increasing the number of the training data. However, effects of bias cannot be balanced-out by increasing the sample size or by repetition (Schmidt et al., 2013).

It is important to describe the target population, which informs the individuals for whom the results of the study are intended to apply. It can be inferred from the data used in the method development. Studies that validated their methods on a dataset different from the one used to develop it, in terms of clinical and image acquisition characteristics, obtained lower spatial agreement in this validation dataset (Roy et al., 2015; Wang et al., 2015; Atlason et al., 2019) (Table 2). Many of the studies included analysed the WMH load in the sample, only expressing that it "was representative of the whole load of WMH burden". However, representativeness does not mean "balanced": unbalanced data biases the results in favour of the dominant data subgroup – generally patients with medium-to-large WMH burden. Also, many studies did not explain the rationale followed for data selection. For instance, patients with mild cognitive impairment, Alzheimer's disease, and normal cognition were included in the same study without explaining the selection criteria and relevance for the main objective of the study, i.e. segmenting WMH. For sample sizes like the ones observed in the majority of studies included (e.g. n<100), cognitive status is not a proxy for WMH load (Damangir et al., 2017). It is, therefore, difficult to decide for which level of severity of a particular condition or for which

neurological condition the segmentation method had performed well and, therefore, would be recommended.

Many of the included studies used the open access datasets or the datasets provided for the different Lesion Segmentation Challenges. Mendelson et al. (2017) pointed out that using an open access dataset to evaluate the performance of a segmentation method introduces selection bias (Mendelson et al., 2017). It, indeed is practical, cost effective and allows comparability between methods, but only within the context of the dataset used, especially in the case of supervised methods. Hence, segmentation studies can suffer from limited high-quality data, which is required for training, and poorly labelled region of interests (Challen et al., 2019). The full value of a large dataset depends on the accuracy and completeness of the data collection, which is expensive and time consuming. The use of a limited dataset in cross-validation can falsely show high performance. To evaluate the performance of a segmentation method, large collections of image data are required. Data augmentation and high quality synthetic data can help addressing this need.

Segmenting a medical image is a laborious task. In general, it requires two main steps: 1) image pre-processing; and 2) segmentation (Jude Hemanth & Anitha, 2012). Pre-processing steps generally involve registration, brain extraction, intensity inhomogeneity correction, noise reduction and intensity normalisation (García-Lorenzo et al., 2013). If task-unrelated pathologies (e.g., stroke lesions, SVD neuroradiological features) or imaging artefacts would affect the segmentation algorithm, their identification should be part of the segmentation framework. Main objectives of pre-processing are removal of noise and confounding features, and improving image quality. Not reporting all these steps can be interpreted as they not being necessary or part of the segmentation framework, affecting its reproducibility. Good reporting quality is extremely important, to ensure that accurate and trustworthy information is obtained from the published studies (Samuel et al., 2016). Quality of reporting research studies needs to be improved by following the guidelines outlined by various organisations ("Reporting guidelines | The EQUATOR Network", 2020).

White Matter Hyperintensities Segmentation Review

Accuracy of the segmentation methods evaluated in this review refers to their ability to distinguish WMH from normal appearing white matter or other pathological features of similar appearance, as well as a reference or "ground truth" segmentation manually generated by experts. Accuracy was estimated with Bland Altman plots, Jaccard Index, intra class correlation coefficient, true and false positives and negatives and DSC. All these measures have advantages and drawbacks when applied to this context, as none of them alone gives the necessary information about the precision and further applicability of the results in a clinical context. For example, the Bland-Altman plot *per-se* only allows volumetric comparison between the target and reference methods. The Jaccard Index and DSC are equivalent and they reflect the spatial agreement between the two masks, but do not express how well the algorithm identified the true WMH and/or excluded the non-WMH voxels, as the true positives and negatives are given by other measurements (e.g., true positive fraction, true negative fraction, positive predicted values, false negative/positive fractions). Finally, the correlation coefficient between quantitative WMH volumes and clinical visual ratings (e.g. Fazekas scores), although of clinical use, only gives a gross estimate of how close to the neuroradiological assessment the segmentation is. Most of the papers included did not analyse the results of these metrics combined. It reinforces the claim by Pellegrini et al. (2018) that the relevant literature of computational segmentation algorithms is still insufficiently intertwined with the clinical world. We believe this depends, at least in part, on a misalignment of targets and methods. The computer scientists' community still aims primarily for algorithm novelty and reaching high levels of precision, experimenting with methods largely inspired by recent developments in the field of computer vision. The clinical research community, on the other hand, aims to verify associations (e.g., biomarkers for outcome, effect of drugs vs. placebo) with clinically relevant features that reflect in an improvement in patient outcomes using statistical models. A combination of methods and aims is, therefore, of great importance. The fact that 22% of the studies analysed incorporated a clinical validation to their scheme is encouraging.

Only 26% of the studies included in the review reported the processing time of the proposed segmentation algorithm. Reporting the processing time of the segmentation method could also

aid in its further translation to clinical practice, by highlighting its speed or the need of optimising its current implementation. Despite its importance, translating research into clinical practice is challenging. Aside from simply demonstrating superior efficacy, new technologies entering the medical field must also integrate with current practices and be effective in an individual case basis. Kristensen et al. (2015) have reported that it takes more than a decade to implement research results in clinical practice. The research required for this "personalised' medicine would only be possible through summarising and integrating enormous quantities of medical information. This review has shown that this is still unachieved.

Strengths and Limitations

This review systematically extracted, synthesised, critically appraised and presents information about a highly active research field. Its main strengths are: 1) careful selection of relevant studies amongst a vast number of initial candidates resultant from the search; 2) identification of the possible sources of bias of the studies; and 3) synthesis of the contributions of the included papers.

Limitations are that we only included the articles published in English language for which we have full access: we may have missed articles published in languages other than English or other articles for which we could not access the full text. Also, there might be other relevant papers missing as a result of incongruences between the search terms and the article keywords or indexing in the databases. By excluding articles published in conference proceedings it is possible that promising WMH segmentation methods could have been excluded.

CONCLUSION AND FUTURE WORKS

Despite the increasing popularity and high accuracy of CNN schemes applied to WMH segmentation, we found no evidence to favour their application in clinical research over the k-NN algorithm, linear regression or unsupervised methods. High-quality large-sized data

availability continues to limit computational developments of segmentation methods, biasing the studies. Future works should carefully consider ways to reduce or compensate the effect of observer, spectrum and selection biases, and improve transparent reporting. Future studies should also analyse the combined effect of several metrics in evaluating the results of their algorithms, to inform on the applicability of the method in clinical research and practice. The lack of code availability of some algorithms presented, and information about the pre- and post-processing steps, and processing time of segmentation *per se* limited the analyses presented and the further reproducibility of the results: issues that we hope future studies overcome.

ACKNOWLEDGEMENTS

MVH is funded by Row Fogo Charitable Trust (Grant no. BROD.FID3668413). This work is supported by: the Row Fogo Centre for Research into Ageing and the Brain, and the UK Dementia Research Institute which receives its funding from DRI Ltd, funded by the UK MRC, Alzheimer's Society and Alzheimer's Research UK. Images were acquired at the Research MR scanners at the Edinburgh Imaging facilities, supported by the Scottish Funding Council through the Scottish Imaging Network, A Platform for Scientific Excellence (SINAPSE) Collaboration; the 3T scanner is funded by the Wellcome Trust (104916/Z/14/Z), Dunhill Trust (R380R/1114), Edinburgh and Lothians Health Foundation (2012/17), Muir Maxwell Research Fund and the University of Edinburgh.

REFERENCES

Advanced Normalization Tools (ANTs) - SourceForge.net. (2020). Retrieved 18 June 2020, from https://sourceforge.net/projects/advants/files/

Anbeek, P., Vincken, K. L., van Osch, M. J., Bisschops, R. H., & van der Grond, J. (2004). Probabilistic segmentation of white matter lesions in MR imaging. *NeuroImage*, *21*(3), 1037–1044. doi: 10.1016/j.neuroimage.2003.10.012

Akudjedu, T. N., Nabulsi, L., Makelyte, M., Scanlon, C., Hehir, S., Casey, H., Ambati, S., Kenney, J., O'Donoghue, S., McDermott, E., Kilmartin, L., Dockery, P., McDonald, C., Hallahan, B., & Cannon, D. M. (2018). A comparative study of segmentation techniques for the quantification of brain subcortical volume. *Brain imaging and behavior*, *12*(6), 1678–1695. doi: 10.1007/s11682-018-9835-y

ANTsX/ANTs. (2020). Retrieved 18 June 2020, from https://github.com/ANTsX/ANTs

Atlason, H. E., Love, A., Sigurdsson, S., Gudnason, V., & Ellingsen, L. M. (2019). SegAE: Unsupervised white matter lesion segmentation from brain MRIs using a CNN autoencoder. *NeuroImage: Clinical*, *24*, 102085. doi: 10.1016/j.nicl.2019.102085

Aubert-Broche, B., Fonov, V., García-Lorenzo, D., Mouiha, A., Guizard, N., & Coupé, P. et al. (2013). A new method for structural volume analysis of longitudinal brain MRI data and its application in studying the growth trajectories of anatomical brain structures in childhood. *Neuroimage*, *82*, 393-402. doi: 10.1016/j.neuroimage.2013.05.065

Ayrignac, X., Menjot de Champfleur, N., Menjot de Champfleur, S., Carra-Dallière, C., Deverdun, J., Corlobe, A., & Labauge, P. (2016). Brain magnetic resonance imaging helps to differentiate atypical multiple sclerosis with cavitary lesions and vanishing white matter disease. *European Journal Of Neurology*, *23*(6), 995-1000. doi: 10.1111/ene.12931

Bauer, S., Nolte, L. P., & Reyes, M. (2011). Skull-stripping for tumour-bearing brain images. Annual Meeting of Swiss Society for Biomedical Engineering (Bern), page 2, Bern, April 2011. SSBE

Blair, G., Valdés Hernández, M., Thrippleton, M., Doubal, F., & Wardlaw, J. (2017). Advanced Neuroimaging of Cerebral Small Vessel Disease. *Current Treatment Options In Cardiovascular Medicine*, *19*(7). doi: 10.1007/s11936-017-0555-1

Bowles, C., Qin, C., Guerrero, R., Gunn, R., Hammers, A., & Dickie, D. et al. (2017). Brain lesion segmentation through image synthesis and outlier detection. *Neuroimage: Clinical*, *16*, 643-658. doi: 10.1016/j.nicl.2017.09.003

Byrne, N., Velasco Forte, M., Tandon, A., Valverde, I., & Hussain, T. (2016). A systematic review of image segmentation methodology, used in the additive manufacture of patient-specific 3D printed models of the cardiovascular system. *JRSM cardiovascular disease*, *5*, 2048004016645467. doi: 10.1177/2048004016645467

Challen, R., Denny, J., Pitt, M., Gompels, L., Edwards, T., & Tsaneva-Atanasova, K. (2019). Artificial intelligence, bias and clinical safety. *BMJ Quality & Safety*, *28*(3), 231-237. doi: 10.1136/bmjqs-2018-008370

Caligiuri, M. E., Perrotta, P., Augimeri, A., Rocca, F., Quattrone, A., & Cherubini, A. (2015). Automatic Detection of White Matter Hyperintensities in Healthy Aging and Pathology Using Magnetic Resonance Imaging: A Review. *Neuroinformatics*, *13*(3), 261–276. doi: 10.1007/s12021-015-9260-y

Cardoso, M. J., Leung, K., Modat, M., Keihaninejad, S., Cash, D., Barnes, J., Fox, N. C., Ourselin, S., & Alzheimer's Disease Neuroimaging Initiative (2013). STEPS: Similarity and Truth Estimation for Propagated Segmentations and its application to hippocampal segmentation and brain parcelation. Medical Image Analysis, 17(6), 671–684. doi: 10.1016/j.media.2013.02.006

Cardoso, M. J., Modat, M., Wolz, R., Melbourne, A., Cash, D., Rueckert, D., & Ourselin, S. (2015). Geodesic information flows: Spatiallyvariant graphs and their application to segmentation and fusion. *IEEE Transactions on Medical Imaging*, 34(9), 1976–1988. doi: 10.1109/TMI.2015.2418298

White Matter Hyperintensities Segmentation Review

Coleman, T., & Li, Y. (1996). An Interior Trust Region Approach for Nonlinear Minimization Subject to Bounds. *SIAM Journal On Optimization*, *6*(2), 418-445. doi: 10.1137/0806023

Coupe, P., Yger, P., Prima, S., Hellier, P., Kervrann, C., Barillot, C. (2008). An optimized blockwise nonlocal means denoising filter for 3-D magnetic resonance images. *IEEE Transactions on Medical Imaging*, 27(4), 425-441. doi:10.1109/TMI.2007.906087

Cox, R. W. (1996). AFNI: software for analysis and visualization of functional magnetic resonance neuroimages. *Computers and Biomedical Research*, 29(3), 162–173. doi: 10.1006/cbmr.1996.0014

Cruz, H., Eckert, M., Meneses, J. M., & Martínez, J. F. (2017). Fast evaluation of segmentation quality with parallel computing. *Scientific Programming*, 1-9. doi: 10.1155/2017/5767521

Dadar, M., Pascoal, T. A., Manitsirikul, S., Misquitta, K., Fonov, V. S., Tartaglia, M. C., Breitner, J., Rosa-Neto, P., Carmichael, O. T., Decarli, C., & Collins, D. L. (2017a). Validation of a Regression Technique for Segmentation of White Matter Hyperintensities in Alzheimer's Disease. *IEEE Transactions on Medical Imaging*, *36*(8), 1758–1768. doi: 10.1109/TMI.2017.2693978

Dadar, M., Maranzano, J., Misquitta, K., Anor, C. J., Fonov, V. S., Tartaglia, M. C., Carmichael, O. T., De Carli, C., Collins, D. L., & Alzheimer's Disease Neuroimaging Initiative (2017b). Performance comparison of 10 different classification techniques in segmenting white matter hyperintensities in aging. *NeuroImage*, *157*, 233–249. doi: 10.1016/j.neuroimage.2017.06.009

Damangir, S., Westman, E., Simmons, A., Vrenken, H., Wahlund, L. O., & Spulber, G. (2017). Reproducible segmentation of white matter hyperintensities using a new statistical definition. *Magma (New York, N.Y.)*, *30*(3), 227–237. doi: 10.1007/s10334-016-0599-3

Debette, S., & Markus, H. (2010). The clinical importance of white matter hyperintensities on brain magnetic resonance imaging: systematic review and meta-analysis. *BMJ*, *341*(jul26 1), c3666-c3666. doi: 10.1136/bmj.c3666

De Boer, R., van der Lijn, F., Vrooman, H., Vernooij, M., Ikram, M., Breteler, M., & Niessen, W. (2007). Automatic Segmentation of Brain Tissue and White Matter Lesions in MRI. *Proceedings of the 2007 IEEE International Symposium on Biomedical Imaging: From Nano to Macro, Washington, DC, USA, April 12-16, 2007*. doi: 10.1109/ISBI.2007.356936

Despotović, I., Goossens, B., & Philips, W. (2015). MRI Segmentation of the Human Brain: Challenges, Methods, and Applications. *Computational and Mathematical Methods In Medicine*, *2015*, 1-23. doi: 10.1155/2015/450341

Ding, T., Cohen, A. D., O'Connor, E. E., Karim, H. T., Crainiceanu, A., Muschelli, J., Lopez, O., Klunk, W. E., Aizenstein, H. J., Krafty, R., Crainiceanu, C. M., & Tudorascu, D. L. (2020). An improved algorithm of white matter hyperintensity detection in elderly adults. *NeuroImage. Clinical*, *25*, 102151. doi: 10.1016/j.nicl.2019.102151

Diniz, P. H. B., Valente, T. L. A., Diniz, J. O. B., Silva, A. C., Gattass, M., Ventura, N., … Gasparetto, E. L. (2018). Detection of white matter lesion regions in MRI using SLIC0 and convolutional neural network. *Computer Methods and Programs in Biomedicine*, *167*, 49-63. doi: 10.1016/j.cmpb.2018.04.011

Documentation/4.10/Training - Slicer Wiki. (2020). Retrieved 18 June 2020, from https://www.slicer.org/wiki/Documentation/UserTraining

EzyFit 2.44. (2020). Retrieved 18 June 2020, from https://www.mathworks.com/matlabcentral/fileexchange/10176-ezyfit-2-44

Fazekas, F., & Wardlaw, J. (2013). The Origin of White Matter Lesions. *Stroke*, *44*(4), 951-952. doi: 10.1161/STROKEAHA.111.000849

Fiford, C. M., Sudre, C. H., Pemberton, H., Walsh, P., Manning, E., Malone, I. B., Nicholas, J., Bouvy, W. H., Carmichael, O. T., Biessels, G. J., Cardoso, M. J., & Barnes, J. (2020). Automated white matter Hyperintensity segmentation using Bayesian model selection: Assessment and

White Matter Hyperintensities Segmentation Review

correlations with cognitive change. *Neuroinformatics*, *18*(3), 429-449. doi: 10.1007/s12021-019-09439-6

FreeSurferWiki - Free Surfer Wiki. (2020). Retrieved 18 June 2020, from https://surfer.nmr.mgh.harvard.edu/fswiki

Gail, M., & Green, S. (1976). Critical Values for the One-Sided Two-Sample Kolmogorov-Smirnov Statistic. *Journal Of The American Statistical Association*, *71*(355), 757-760. doi: 10.1080/01621459.1976.10481562

García-Lorenzo, D., Francis, S., Narayanan, S., Arnold, D. L., & Collins, D. L. (2013). Review of automatic segmentation methods of multiple sclerosis white matter lesions on conventional magnetic resonance imaging. *Medical Image Analysis*, *17*(1), 1–18. doi: 10.1016/j.media.2012.09.004

Ghafoorian, M., Karssemeijer, N., Heskes, T., van Uden, I., Sanchez, C. I., Litjens, G., de Leeuw, F. E., van Ginneken, B., Marchiori, E., & Platel, B. (2017). Location Sensitive Deep Convolutional Neural Networks for Segmentation of White Matter Hyperintensities. *Scientific Reports*, *7*(1), 5110. doi: 10.1038/s41598-017-05300-5

Griffanti, L., Zamboni, G., Khan, A., Li, L., Bonifacio, G., Sundaresan, V., Schulz, U. G., Kuker, W., Battaglini, M., Rothwell, P. M., & Jenkinson, M. (2016). BIANCA (Brain Intensity AbNormality Classification Algorithm): A new tool for automated segmentation of white matter hyperintensities. *NeuroImage*, *141*, 191–205. doi: 10.1016/j.neuroimage.2016.07.018

Guerrero, R., Qin, C., Oktay, O., Bowles, C., Chen, L., Joules, R., Wolz, R., Valdés-Hernández, M. C., Dickie, D. A., Wardlaw, J., & Rueckert, D. (2017). White matter hyperintensity and stroke lesion segmentation and differentiation using convolutional neural networks. *NeuroImage. Clinical*, *17*, 918–934. doi: 10.1016/j.nicl.2017.12.022

Hachinski, V.C., Potter, P., & Merskey, H. (1987) Leuko-araiosis. Archives of Neurology, 44(1), 21-3. doi: 10.1001/archneur.1987.00520130013009

Haralick, R., Shapiro, L. (1991). Glossary of computer vision terms. *Pattern Recognition*, 24(1), 69-93. doi: 10.1016/0031-3203(91)90117-n

Hasan, T. F., Barrett, K. M., Brott, T. G., Badi, M. K., Lesser, E. R., Hodge, D. O., & Meschia, J. F. (2019). Severity of White Matter Hyperintensities and Effects on All-Cause Mortality in the Mayo Clinic Florida Familial Cerebrovascular Diseases Registry. *Mayo Clinic Proceedings*, *94*(3), 408–416. doi: 10.1016/j.mayocp.2018.10.024

Heckemann, R. A., Ledig, C., Gray, K. R., Aljabar, P., Rueckert, D., Hajnal, J. V., & Hammers, A. (2015). Brain Extraction Using Label Propagation and Group Agreement: Pincram. *Plos One, 10*(7). doi: 10.1371/journal.pone.0129211

Hong, J., Park, B., Lee, M. J., Chung, C., Cha, J., & Park, H. (2020). Two-step deep neural network for segmentation of deep white matter hyperintensities in migraineurs. *Computer Methods and Programs in Biomedicine*, *183*, 105065. doi: 10.1016/j.cmpb.2019.105065

Huppertz H.-J., Wagner J., Weber B., House P., Urbach H. (2011). Automated quantitative FLAIR analysis in hippocampal sclerosis. *Epilepsy Research*, 97, 146-156. doi: 10.1016/j.eplepsyres.2011.08.001

Imaging in COVID-19 complications - ESR Connect. (2020). Retrieved 14 June 2020, from https://connect.myesr.org/course/imaging-in-covid-19-complications/

Inzitari, D. (2003). Leukoaraiosis. *Stroke*, *34*(8), 2067-2071. doi: 10.1161/01.STR.0000080934.68280.82

Jenkinson, M., & Smith, S. (2001). A global optimisation method for robust affine registration of brain images. *Medical Image Analysis*, *5*(2), 143–156. doi: 10.1016/s1361-8415(01)00036-6

Jenkinson, M., Bannister, P., Brady, M., & Smith, S. (2002). Improved optimization for the robust and accurate linear registration and motion correction of brain images. *NeuroImage*, *17*(2), 825–841. doi: 10.1016/s1053-8119(02)91132-8

Jenkinson, M., Pechaud, M., Smith, S.,M. (2004). BET2: MR-based estimation of brain, skull and scalp surfaces. *Eleventh Annual Meeting of the Organization for Human Brain Mapping, Toronto, Ontario*, p. 716

Jiang, J., Liu, T., Zhu, W., Koncz, R., Liu, H., Lee, T., Sachdev, P. S., & Wen, W. (2018). UBO Detector - A cluster-based, fully automated pipeline for extracting white matter hyperintensities. *NeuroImage*, *174*, 539–549. doi: 10.1016/j.neuroimage.2018.03.050

Jude Hemanth, D., & Anitha, J. (2012). Image Pre-processing and Feature Extraction Techniques for Magnetic Resonance Brain Image Analysis. *Communications in Computer and Information Science*, 349-356. doi: 10.1007/978-3-642-35594-3_47

Kamnitsas, K., Ledig, C., Newcombe, V., Simpson, J. P., Kane, A. D., Menon, D. K., Rueckert, D., & Glocker, B. (2017). Efficient multi-scale 3D CNN with fully connected CRF for accurate brain lesion segmentation. *Medical Image Analysis*, *36*, 61–78. doi: 10.1016/j.media.2016.10.004

Keller, S. S., & Roberts, N. (2009). Measurement of brain volume using MRI: software, techniques, choices and prerequisites. *Journal of anthropological sciences = Rivista di antropologia : JASS*, *87*, 127–151.

Kim, K. W., MacFall, J. R., & Payne, M. E. (2008). Classification of white matter lesions on magnetic resonance imaging in elderly persons. *Biological psychiatry*, *64*(4), 273–280. doi: 10.1016/j.biopsych.2008.03.024

Klein, S., Staring, M., Murphy, K., Viergever, M. A., & Pluim, J. P. (2010). elastix: a toolbox for intensity-based medical image registration. *IEEE Transactions on Medical Imaging*, *29*(1), 196–205. doi: 10.1109/TMI.2009.2035616

Knight, J., Taylor, G., & Khademi, A. (2018). Voxel-Wise Logistic Regression and Leave-One-Source-Out Cross Validation for white matter hyperintensity segmentation. *Magnetic Resonance Imaging*, *54*, 119-136. doi: 10.1016/j.mri.2018.06.009

Kristensen, N., Nymann, C., & Konradsen, H. (2015). Implementing research results in clinical practice- the experiences of healthcare professionals. *BMC Health Services Research*, *16*(1). doi: 10.1186/s12913-016-1292-y

Kuijf, H. J., Biesbroek, J. M., De Bresser, J., Heinen, R., Andermatt, S., Bento, M., Berseth, M., *et al.* (2019). Standardized Assessment of Automatic Segmentation of White Matter Hyperintensities and Results of the WMH Segmentation Challenge. *IEEE Transactions on Medical Imaging*, *38*(11), 2556–2568. doi: 10.1109/TMI.2019.2905770

Kwan, R. K. S., Evans, A. C., & Pike, B. (1999). MRI simulation-based evaluation of image-processing and classification methods. *IEEE Transactions on Medical Imaging*, 18 (11), 1085–1097. doi: 10.1109/42.816072

Labauge, P., Horzinski, L., Ayrignac, X., Blanc, P., Vukusic, S., Rodriguez, D., Mauguiere, F., *et al.* (2009). Natural history of adult-onset eIF2B-related disorders: a multi-centric survey of 16 cases. *Brain : a journal of neurology*, *132*(Pt 8), 2161–2169. doi: 10.1093/brain/awp171

Li, H., Jiang, G., Zhang, J., Wang, R., Wang, Z., Zheng, W. S., & Menze, B. (2018). Fully convolutional network ensembles for white matter hyperintensities segmentation in MR images. *NeuroImage*, *183*, 650–665. doi: 10.1016/j.neuroimage.2018.07.005

Liu, W., Hua, G., & Smith, J. (2014). Unsupervised One-Class Learning for Automatic Outlier Removal. *2014 IEEE Conference On Computer Vision And Pattern Recognition*. doi: 10.1109/cvpr.2014.483

Ling, Y., Jouvent, E., Cousyn, L., Chabriat, H., & De Guio, F. (2018). Validation and Optimization of BIANCA for the Segmentation of Extensive White Matter Hyperintensties. *Neuroinformatics*, *16*(2), 269–281. doi: 10.1007/s12021-018-9372-2

Liu, L., Chen, S., Zhu, X., Zhao, X., Wu, F., & Wang, J. (2020). Deep convolutional neural network for accurate segmentation and quantification of white matter hyperintensities. *Neurocomputing*, *384*, 231-242. doi: 10.1016/j.neucom.2019.12.050

Lladó, X., Ganiler, O., Oliver, A., Martí, R., Freixenet, J., & Valls, L. et al. (2011). Automated detection of multiple sclerosis lesions in serial brain MRI. *Neuroradiology*, *54*(8), 787-807. doi: 10.1007/s00234-011-0992-6

Llado, X., Oliver, A., Cabezas, M., Freixenet, J., Vilanova, J. C., Quiles, A., Valls, L., Ramió-Torrentà, Ll., Rovira, A. (2012). Segmentation of multiple sclerosis lesions in brain MRI: A review of automated approaches. *Information Sciences,* 186, 164-185. doi: 10.1016/j.ins.2011.10.011

Lutkenhoff, E., Rosenberg, M., Chiang, J., Zhang, K., Pickard, J., Owen, A., & Monti, M. (2014). Optimized Brain Extraction for Pathological Brains (optiBET). *Plos ONE*, *9*(12), e115551. doi: 10.1371/journal.pone.0115551

Maino, G., & Foresti, G. (2011). *Image analysis and processing--ICIAP 2011*. Heidelberg: Springer. doi: 10.1007/978-3-642-24085-0

Maltais, M., de Souto Barreto, P., Moon, S. Y., Rolland, Y., Vellas, B., & MAPT/DSA Study Group (2019). Prospective association of white matter hyperintensity volume and frailty in older adults. *Experimental gerontology*, *118*, 51–54. doi: 10.1016/j.exger.2019.01.007

Maniega, S. M., Valdés Hernández, M. C., Clayden, J. D., Royle, N. A., Murray, C., Morris, Z., Aribisala, B. S., Gow, A. J., Starr, J. M., Bastin, M. E., Deary, I. J., & Wardlaw, J. M. (2015). White matter hyperintensities and normal-appearing white matter integrity in the aging brain. *Neurobiology of aging*, *36*(2), 909–918. doi: 10.1016/j.neurobiolaging.2014.07.048

Manjón, J. V., Coupé, P., Martí-Bonmatí, L., Collins, D. L., & Robles, M. (2010). Adaptive non-local means denoising of MR images with spatially varying noise levels. *Journal of magnetic resonance imaging : JMRI*, *31*(1), 192–203. doi: 10.1002/jmri.22003

Manjón, J. V., Coupé, P., Raniga, P., Xia, Y., Desmond, P., Fripp, J., & Salvado, O. (2018). MRI white matter lesion segmentation using an ensemble of neural networks and overcomplete patch-based voting. *Computerized Medical Imaging and Graphics : the official journal of the Computerized Medical Imaging Society*, *69*, 43–51. doi: 10.1016/j.compmedimag.2018.05.001

Martin Bland, J., & Altman, D. (1986). Statistical methods for assessing agreement between two methods of clinical measurement. *The Lancet*, 1 (8476), 307-310.

Mendelson, A., Zuluaga, M., Lorenzi, M., Hutton, B., & Ourselin, S. (2017). Selection bias in the reported performances of AD classification pipelines. *Neuroimage: Clinical*, *14*, 400-416. doi: 10.1016/j.nicl.2016.12.018

Miller, D. H., Grossman, R. I., Reingold, S. C., & McFarland, H. F. (1998). The role of magnetic resonance techniques in understanding and managing multiple sclerosis. *Brain : a journal of neurology*, *121 (Pt 1)*, 3–24. doi: 10.1093/brain/121.1.3

MIRTK – BioMedIA. (2020). Retrieved 18 June 2020, from https://biomedia.doc.ic.ac.uk/software/mirtk/

Modat, M., Cash, D. M., Daga, P., Winston, G. P., Duncan, J. S., & Ourselin, S. (2014). Global image registration using a symmetric block-matching approach. *Journal of medical imaging (Bellingham, Wash.)*, *1*(2), 024003. doi: 10.1117/1.JMI.1.2.024003

White Matter Hyperintensities Segmentation Review

Mortazavi, D., Kouzani, A. Z., & Soltanian-Zadeh, H. (2012). Segmentation of multiple sclerosis lesions in MR images: a review. *Neuroradiology*, *54*(4), 299–320. doi: 10.1007/s00234-011-0886-7

Moeskops, P., Viergever, M., Mendrik, A., de Vries, L., Benders, M., & Isgum, I. (2016). Automatic Segmentation of MR Brain Images With a Convolutional Neural Network. *IEEE Transactions On Medical Imaging*, *35*(5), 1252-1261.

Moeskops, P., Bresser, J. D., Kuijf, H. J., Mendrik, A. M., Biessels, G. J., Pluim, J. P., & Išgum, I. (2018). Evaluation of a deep learning approach for the segmentation of brain tissues and white matter hyperintensities of presumed vascular origin in MRI. *NeuroImage: Clinical*, *17*, 251–262. doi: 10.1109/TMI.2016.2548501

MRI Shows Brain Abnormalities in Some COVID-19 Patients. (2020). Retrieved 14 June 2020, from https://www.diagnosticimaging.com/covid-19/mri-shows-brain-abnormalities-some-covid-19-patients

Muschelli, J., Gherman, A., Fortin, J. P., Avants, B., Whitcher, B., Clayden, J. D., Caffo, B. S., & Crainiceanu, C. M. (2019). Neuroconductor: an R platform for medical imaging analysis. Biostatistics (Oxford, England), 20(2), 218–239. doi: 10.1093/biostatistics/kxx068

NITRC: MRIcron: Document Manager: Display Document. (2020). Retrieved 18 June 2020, from https://www.nitrc.org/docman/?group_id=152

Nyúl, L. G., & Udupa, J. K. (1999). On standardizing the MR image intensity scale. *Magnetic Resonance in Medicine*, *42*(6), 1072–1081. doi: 10.1002/(sici)1522-2594(199912)42:6<1072::aid-mrm11>3.0.co;2-m

Park, B. Y., Lee, M. J., Lee, S. H., Cha, J., Chung, C. S., Kim, S. T., & Park, H. (2018). DEWS (DEep White matter hyperintensity Segmentation framework): A fully automated pipeline for

detecting small deep white matter hyperintensities in migraineurs. *NeuroImage. Clinical*, *18*, 638–647. doi: 10.1016/j.nicl.2018.02.033

Pellegrini, E., Ballerini, L., Hernandez, M., Chappell, F. M., González-Castro, V., Anblagan, D., Danso, S., Muñoz-Maniega, S., Job, D., Pernet, C., Mair, G., MacGillivray, T. J., Trucco, E., & Wardlaw, J. M. (2018). Machine learning of neuroimaging for assisted diagnosis of cognitive impairment and dementia: A systematic review. *Alzheimer's & dementia (Amsterdam, Netherlands)*, *10*, 519–535. doi: 10.1016/j.dadm.2018.07.004

Qin, C., Guerrero, R., Bowles, C., Chen, L., Dickie, D., & Valdes-Hernandez, M. et al. (2018). A large margin algorithm for automated segmentation of white matter hyperintensity. *Pattern Recognition*, *77*, 150-159. doi: 10.1016/j.patcog.2017.12.016

Rachmadi, M. F., Valdés-Hernández, M. D., Li, H., Guerrero, R., Meijboom, R., Wiseman, S., Waldman, A., Zhang, J., Rueckert, D., Wardlaw, J., & Komura, T. (2020). Limited one-time sampling irregularity map (LOTS-IM) for automatic unsupervised assessment of white matter Hyperintensities and multiple sclerosis lesions in structural brain magnetic resonance images. *Computerized Medical Imaging and Graphics*, *79*, 101685. doi: 10.1016/j.compmedimag.2019.101685

Rachmadi, M. F., Valdés-Hernández, M., Agan, M., Di Perri, C., Komura, T., & Alzheimer's Disease Neuroimaging Initiative (2018). Segmentation of white matter hyperintensities using convolutional neural networks with global spatial information in routine clinical brain MRI with none or mild vascular pathology. *Computerized medical imaging and graphics: the official journal of the Computerized Medical Imaging Society*, *66*, 28–43. doi: 10.1016/j.compmedimag.2018.02.002

Rachmadi, M., Valdés-Hernández, M., Agan, M., & Komura, T. (2017). Deep Learning vs. Conventional Machine Learning: Pilot Study of WMH Segmentation in Brain MRI with Absence or Mild Vascular Pathology. *Journal Of Imaging*, *3*(4), 66. doi: 10.3390/jimaging3040066

White Matter Hyperintensities Segmentation Review

Reporting guidelines | The EQUATOR Network. (2020). Retrieved 5 July 2020, from https://www.equator-network.org/reporting-guidelines/

Rincón, M., Díaz-López, E., Selnes, P., Vegge, K., Altmann, M., Fladby, T., & Bjørnerud, A. (2017). Improved Automatic Segmentation of White Matter Hyperintensities in MRI Based on Multilevel Lesion Features. *Neuroinformatics*, *15*(3), 231–245. doi: 10.1007/s12021-017-9328-y

Roy, P., Bhuiyan, A., Janke, A., Desmond, P., Wong, T-Y., Abhayaratna, W., & Ramamohanarao, K. (2015). Automatic white matter lesion segmentation using contrast enhanced FLAIR intensity and Markov Random Field. *Computerized Medical Imaging and Graphics*. 45. doi: 10.1016/j.compmedimag.2015.08.005.

Roy, S., Butman, J. A., Pham, D. L., & Alzheimers Disease Neuroimaging Initiative (2017). Robust skull stripping using multiple MR image contrasts insensitive to pathology. NeuroImage, 146, 132–147. doi: 10.1016/j.neuroimage.2016.11.017

Samuel, G., Hoffmann, S., Wright, R., Lalu, M., Patlewicz, G., & Becker, R. et al. (2016). Guidance on assessing the methodological and reporting quality of toxicologically relevant studies: A scoping review. *Environment International*, *92-93*, 630-646. doi: 10.1016/j.envint.2016.03.010

Schirmer, M. D., Dalca, A. V., Sridharan, R., Giese, A. K., Donahue, K. L., Nardin, M. J., Mocking, S., McIntosh, E. C., Frid, P., Wasselius, J., Cole, J. W., Holmegaard, L., Jern, C., Jimenez-Conde, J., Lemmens, R., Lindgren, A. G., Meschia, J. F., Roquer, J., Rundek, T., Sacco, R. L., …, MRI-GENIE Investigators (2019). White matter hyperintensity quantification in large-scale clinical acute ischemic stroke cohorts - The MRI-GENIE study. *NeuroImage. Clinical*, *23*, 101884. doi: 10.1016/j.nicl.2019.101884

Schmidt, R. L., & Factor, R. E. (2013). Understanding sources of bias in diagnostic accuracy studies. *Archives of pathology & laboratory medicine*, *137*(4), 558–565. doi: 10.5858/arpa.2012-0198-RA

Shamonin, D. P., Bron, E. E., Lelieveldt, B. P., Smits, M., Klein, S., Staring, M., & Alzheimer's Disease Neuroimaging Initiative (2014). Fast parallel image registration on CPU and GPU for diagnostic classification of Alzheimer's disease. *Frontiers in neuroinformatics*, *7*, 50. doi: 10.3389/fninf.2013.00050

Shinohara, R. T., Goldsmith, J., Mateen, F. J., Crainiceanu, C., & Reich, D. S. (2012). Predicting breakdown of the blood-brain barrier in multiple sclerosis without contrast agents. *AJNR. American journal of neuroradiology*, *33*(8), 1586–1590. doi: 10.3174/ajnr.A2997

Sled, J. G., Zijdenbos, A. P., & Evans, A. C. (1998). A nonparametric method for automatic correction of intensity nonuniformity in MRI data. *IEEE transactions on medical imaging*, *17*(1), 87–97. doi: 10.1109/42.668698

Smith, S. (2002). Fast robust automated brain extraction. *Human Brain Mapping*, *17*(3), 143-155. doi: 10.1002/hbm.10062

SPM - Documentation. (2020). Retrieved 18 June 2020, from https://www.fil.ion.ucl.ac.uk/spm/doc/

Steenwijk, M. D., Pouwels, P. J., Daams, M., van Dalen, J. W., Caan, M. W., Richard, E., Barkhof, F., & Vrenken, H. (2013). Accurate white matter lesion segmentation by k nearest neighbor classification with tissue type priors (kNN-TTPs). *NeuroImage. Clinical*, *3*, 462–469. doi: 10.1016/j.nicl.2013.10.003

Stone, J. R., Wilde, E. A., Taylor, B. A., Tate, D. F., Levin, H., Bigler, E. D., Scheibel, R. S., Newsome, M. R., Mayer, A. R., Abildskov, T., Black, G. M., Lennon, M. J., York, G. E., Agarwal, R., DeVillasante, J., Ritter, J. L., Walker, P. B., Ahlers, S. T., & Tustison, N. J. (2016). Supervised learning technique for the automated identification of white matter hyperintensities in traumatic brain injury. *Brain injury*, *30*(12), 1458–1468. doi: 10.1080/02699052.2016.1222080

White Matter Hyperintensities Segmentation Review

Styner, M., Lee, J., Chin, B., Chin, M., Commowick, O., Tran, H-H., Jewells, V., & Warfield, S. (2007). 3D segmentation in the clinic: A grand challenge II: MS lesion segmentation. MIDAS Journal. Accessed 20 June 2020 from http://hdl.handle.net/10380/1449

Sudre, C. H., Cardoso, M. J., Bouvy, W. H., Biessels, G. J., Barnes, J., & Ourselin, S. (2015). Bayesian model selection for pathological neuroimaging data applied to white matter lesion segmentation. *IEEE Transactions on Medical Imaging*, 34(10), 2079–2102. doi: 10.1109/TMI.2015.2419072

Sudre, C. H., Cardoso, M. J., Ourselin, S., & Alzheimer's Disease Neuroimaging Initiative (2017). Longitudinal segmentation of age-related white matter hyperintensities. *Medical Image Analysis*, 38, 50–64. doi: 10.1016/j.media.2017.02.007

Sundaresan, V., Zamboni, G., Le Heron, C., Rothwell, P., Husain, M., & Battaglini, M. et al. (2019). Automated lesion segmentation with BIANCA: Impact of population-level features, classification algorithm and locally adaptive thresholding. *Neuroimage*, *202*, 116056. doi: 10.1016/j.neuroimage.2019.116056

Sweeney, E. M., Shinohara, R. T., Shiee, N., Mateen, F. J., Chudgar, A. A., Cuzzocreo, J. L., Calabresi, P. A., Pham, D. L., Reich, D. S., & Crainiceanu, C. M. (2013). OASIS is automated statistical inference for segmentation, with applications to multiple sclerosis lesion segmentation in MRI. *NeuroImage: Clinical*, 2, 402-413. doi: 10.1016/j.nicl.2013.03.002

Valdés Hernández, M.C., Ferguson, K. J., Chappell, F. M., Wardlaw, J. M. (2010). New multispectral MRI data fusion technique for white matter lesion segmentation: method and comparison with thresholding in FLAIR images. *European Radiology*, 20(7), 1684-1691. doi: 10.1007/s00330-010-1718-6

Valverde, S., Oliver, A., Roura, E., González-Villà, S., Pareto, D., Vilanova, J. C., Ramió-Torrentà, L., Rovira, À., & Lladó, X. (2017). Automated tissue segmentation of MR brain images in the

presence of white matter lesions. Medical image analysis, 35, 446–457. doi: 10.1016/j.media.2016.08.014

Van Leemput, K., Maes, F., Vandermeulen, D., & Suetens, P. (1999).Automated model-based tissue classification of MR images of the brain. IEEE Transactions on Medical Imaging, 18(10), 897–908. doi: 10.1109/42.811270

Van Opbroek, A., Ikram, M., Vernooij, M., & de Bruijne, M. (2015a). Transfer Learning Improves Supervised Image Segmentation Across Imaging Protocols. *IEEE Transactions On Medical Imaging*, *34*(5), 1018-1030. doi: 10.1109/TMI.2014.2366792

Van Opbroek, A. V., Vernooij, M. W., Ikram, M. A., & Bruijne, M. (2015b). Weighting training images by maximizing distribution similarity for supervised segmentation across scanners. *Medical image analysis*, *24*(1), 245–254. doi: 10.1016/j.media.2015.06.010

 "VisibleHuman.png." *MRIcro | CRNL*, www.mccauslandcenter.sc.edu/crnl/mricro.

Viola, P., Wells III, W. M. (1997) Alignment by maximization of mutual information. *IntJ Comput Vis*, 24(2), 137-154. doi: 10.1109/ICCV.1995.466930

Wang, R., Li, C., Wang, J., Wei, X., Li, Y., Zhu, Y., & Zhang, S. (2015). Automatic segmentation and volumetric quantification of white matter hyperintensities on fluid-attenuated inversion recovery images using the extreme value distribution. *Neuroradiology*, *57*(3), 307–320. doi: 10.1007/s00234-014-1466-4

Warfield, S., Kaus, M., Jolesz, F., & Kikinis, R. (2000). Adaptive, template moderated, spatially varying statistical classification. *Medical Image Analysis*, *4*(1), 43-55. doi: 10.1016/s1361-8415(00)00003-7

Wardlaw, J. M., Smith, E. E., Biessels, G. J., Cordonnier, C., Fazekas, F., Frayne, R., Lindley, R. I., O'Brien, J. T., Barkhof, F., Benavente, O. R., Black, S. E., Brayne, C., Breteler, M., Chabriat, H., Decarli, C., de Leeuw, F. E., Doubal, F., Duering, M., Fox, N. C., Greenberg, S., … STandards for

ReportIng Vascular changes on nEuroimaging (STRIVE v1) (2013). Neuroimaging standards for research into small vessel disease and its contribution to ageing and neurodegeneration. *The Lancet. Neurology*, *12*(8), 822–838. doi: 10.1016/S1474-4422(13)70124-8

Wardlaw, J., Valdés Hernández, M., & Muñoz-Maniega, S. (2015). What are White Matter Hyperintensities Made of?. *Journal Of The American Heart Association*, *4*(6). doi: 10.1161/JAHA.114.001140

Wu, Y., & Liu, Y. (2013). Adaptively Weighted Large Margin Classifiers. *Journal Of Computational And Graphical Statistics*, *22*(2), 416-432. doi: 10.1080/10618600.2012.680866

Wu, J., Zhang, Y., Wang, K., & Tang, X. (2019). Skip connection U-net for white matter Hyperintensities segmentation from MRI. IEEE Access, 7, 155194-155202. doi: 10.1109/access.2019.2948476

Wu, D., Albert, M., Soldan, A., Pettigrew, C., Oishi, K., Tomogane, Y., Ye, C., Ma, T., Miller, M. I., & Mori, S. (2019). Multi-atlas based detection and localization (MADL) for location-dependent quantification of white matter hyperintensities. *NeuroImage. Clinical*, *22*, 101772. doi: 10.1016/j.nicl.2019.101772

Zhang, Y., Brady, M., & Smith, S. (2001). Segmentation of brain MR images through a hidden Markov random field model and the expectation-maximization algorithm. *IEEE transactions on medical imaging*, *20*(1), 45–57. doi: 10.1109/42.906424

Zhan, T., Liu, Z., Xiao, L., Zhan, Y., & Wei, Z. (2015). Automatic method for white matter lesion segmentation based on T1-fluid-attenuated inversion recovery images. *IET Computer Vision*, *9*(4), 447–455. doi: 10.1049/iet-cvi.2014.0121

 Zhan, T., Yu, R., Zheng, Y., Zhan, Y., Xiao, L. and Wei, Z., 2017. Multimodal spatial-based segmentation framework for white matter lesions in multi-sequence magnetic resonance

images. *Biomedical Signal Processing and Control*, 31, pp.52-62. doi: 10.1016/j.bspc.2016.06.016

Zheng, J., Delbaere, K., Close, J., Sachdev, P., & Lord, S. (2011). Impact of White Matter Lesions on Physical Functioning and Fall Risk in Older People. *Stroke*, *42*(7), 2086-2090. doi: 10.1161/strokeaha.110.610360